

PAPER • OPEN ACCESS

Simultaneous energy and mass calibration of large-radius jets with the ATLAS detector using a deep neural network

To cite this article: G Aad *et al* 2024 *Mach. Learn.: Sci. Technol.* **5** 035051

View the [article online](#) for updates and enhancements.

You may also like

- [Etching of Ga₂O₃: an important process for device manufacturing](#)
Zhaoying Xi, Zeng Liu, Junpeng Fang et al.
- [Design of systems for plasma activated water \(PAW\) for agri-food applications](#)
N N Misra, Tejas Naladala and Khalid J Alzahrani
- [A ⁸⁵Rb transverse modulation magnetometer in the geophysical range based on atomic alignment states](#)
Tao Shi, Ge Jin, Hong Zhang et al.



PAPER

Simultaneous energy and mass calibration of large-radius jets with the ATLAS detector using a deep neural network

OPEN ACCESS

RECEIVED
7 December 2023REVISED
17 April 2024ACCEPTED FOR PUBLICATION
9 July 2024PUBLISHED
3 September 2024

Original Content from this work may be used under the terms of the [Creative Commons Attribution 4.0 licence](https://creativecommons.org/licenses/by/4.0/).

Any further distribution of this work must maintain attribution to the author(s) and the title of the work, journal citation and DOI.



The ATLAS Collaboration

E-mail: gabriela.navarro@uan.edu.co

Keywords: ATLAS, detector, CERN jets, calibrations

Abstract

The energy and mass measurements of jets are crucial tasks for the Large Hadron Collider experiments. This paper presents a new calibration method to simultaneously calibrate these quantities for large-radius jets measured with the ATLAS detector using a deep neural network (DNN). To address the specificities of the calibration problem, special loss functions and training procedures are employed, and a complex network architecture, which includes feature annotation and residual connection layers, is used. The DNN-based calibration is compared to the standard numerical approach in an extensive series of tests. The DNN approach is found to perform significantly better in almost all of the tests and over most of the relevant kinematic phase space. In particular, it consistently improves the energy and mass resolutions, with a 30% better energy resolution obtained for transverse momenta $p_T > 500$ GeV.

Contents

1. Introduction	2
2. The ATLAS detector	3
3. Jets and their calibration with the ATLAS detector	3
4. Samples and selections	5
4.1. Event simulation	5
4.2. Jet reconstruction and selection	6
5. Methodology of the deep neural network calibration	6
5.1. Loss function	7
5.2. Input features	8
5.3. Architecture	9
5.4. Training procedure	10
6. Performance and validation of the calibration	11
6.1. Technical performance	11
6.2. Calibration performance	11
6.2.1. Performance on QCD dijets	12
6.2.2. Effect of η annotation	12
6.2.3. Performance on other topologies	13
6.3. Validation of the DNN calibration	15
6.3.1. Spectrum dependency	15
6.3.2. Pile-up dependency	16
6.3.3. Jet flavour dependence	17
6.3.4. Dependency on the generator	17
7. Limitations and possible solutions	19
7.1. Training convergence and ending criterion	19
7.2. Calibration of heavy boosted jets	20
7.3. Importance of the features	20
8. Conclusion	21
Data availability statement	21
Acknowledgments	22
References	36

1. Introduction

Jets—the collimated sprays of hadrons resulting from a high momentum quark or gluon emission—are abundantly produced during the operation of the Large Hadron Collider (LHC). They are relevant to almost all physics analyses of the collisions recorded by the LHC experiments, either because they are part of the final state of the studied signal or because they generate background for the process of interest. To achieve high-quality physics results, it is crucial to precisely measure the angular position and energy of the jets. This task is made difficult by multiple effects including fluctuations in the parton showers or in the interactions between the particles forming the jets and the detectors [1]. Another important task is to measure the collimated hadronic decay of high-momentum heavy particles such as top quarks, W , Z or Higgs bosons. These are reconstructed as jets with large angular opening (large- R jets) and the measurement of their mass as well as their energy is therefore necessary.

To measure the jet energy and mass from raw detector signals, the ATLAS and CMS collaborations use calibration procedures comprising multiple steps [2, 3]. In these procedures, the main energy and mass corrections are evaluated numerically from simulated collision events. The corrections are evaluated and applied in two distinct successive steps, in bins of a limited (usually two or three) number of characteristic variables. However, calibrating both highly correlated energy and mass while exploiting all shower variables and their correlations in a single correction step is possible through approaches based on deep neural networks (DNN). This paper presents a full implementation developed by the ATLAS Collaboration using 13 TeV simulated collision events, overcoming several difficulties that are specific to the calibration problem. This new calibration method aims at replacing the current simulation-based corrections of the energy and mass of large- R jets. After a brief introduction to the ATLAS detector (section 2), the paper explains why jet energy and mass calibrations are necessary, reviews the current procedure in ATLAS and motivates the new DNN approach (section 3). The samples used and the selections applied to them are described in section 4. Section 5 details the specific methodology needed to construct and properly train the network, while section 6 discusses the validation and performance of the resulting DNN calibration, comparing it with the

current numerical method. Finally section 7 identifies and discusses limitations in this approach as well as some possible solutions.

2. The ATLAS detector

The ATLAS detector [4] covers nearly the entire solid angle around the collision point¹. It consists of an inner tracking detector surrounded by a thin superconducting solenoid, electromagnetic and hadron calorimeters, and a muon spectrometer incorporating three large superconducting air-core toroidal magnets.

The inner-detector system (ID) is immersed in a 2 T axial magnetic field and provides charged-particle tracking in the range of $|\eta| < 2.5$. The high-granularity silicon pixel detector covers the vertex region and typically provides four measurements per track, the first hit normally being in the insertable B-layer (IBL) [5, 6] installed before Run 2 of the LHC. It is followed by the silicon microstrip tracker (SCT), which usually provides eight measurements per track. These silicon detectors are complemented by the transition radiation tracker (TRT), which enables radially extended track reconstruction up to $|\eta| = 2.0$. The TRT also provides electron identification information based on the fraction of hits (typically 30 in total) above a higher energy-deposit threshold corresponding to transition radiation.

The calorimeter system covers the pseudorapidity range of $|\eta| < 4.9$. In the region $|\eta| < 3.2$, electromagnetic calorimetry is provided by barrel and endcap high-granularity lead/liquid-argon (LAr) calorimeters, with an additional thin LAr presampler covering $|\eta| < 1.8$ to correct for energy loss in material upstream of the calorimeters. Hadron calorimetry is provided by the steel/scintillator-tile calorimeter, segmented into three barrel structures with $|\eta| < 1.7$, and two copper/LAr hadron endcap calorimeters. The solid angle coverage is completed with forward copper/LAr and tungsten/LAr calorimeter modules optimised for electromagnetic and hadronic energy measurements respectively.

The angular and longitudinal segmentation of the calorimeters provides valuable 3-dimensional information about the location of the energy deposits. This allows the calculation of quantities useful for the characterization of the energy shower resulting from various type of particles or groups of particles such as hadronic jets.

An extensive software suite [7] is used in data simulation, in the reconstruction and analysis of real and simulated data, in detector operations, and in the trigger and data acquisition systems of the experiment.

3. Jets and their calibration with the ATLAS detector

After the parton emission, the complete hadronisation process results in a set of particles from which the *particle jets* are formed. These are also named *true jets* in the context of simulated events discussed in this paper. In practice the group of particles forming a true jet, its constituents, is obtained by applying a physically motivated procedure called a jet clustering algorithm on the set of kinematic 4-vectors of all the stable interacting particles of the collision (details are given in section 4.1). The sum of the 4-vectors of a jet's constituents defines its momentum and thus the *true jet* energy and mass. These are the reference quantities for the jet calibration that is applied to experimental jets reconstructed with the ATLAS detector. Jet reconstruction is based on two types of primary signals: charged particle tracks, which are reconstructed from measurements of hits in the inner detector [8, 9] and topological clusters, which are reconstructed from energy deposits in the calorimeters [10]. Tracks and clusters can then be combined to form higher-level objects, each characterised by a kinetic 4-vector [11, 12]. Together, these objects approximate the flow of hadronic particles and are used as the constituents of the reconstructed jets. The final jets are obtained by regrouping these constituents using the same jet algorithm as used for the true jets.

Due to various detector inefficiencies and limitations, the kinematics of the experimentally reconstructed jets differ significantly from the corresponding true jets. Precise and complex corrections are thus applied to the jet energy and mass before these quantities are used in physics analyses [2]. These corrections are separated into two steps. Firstly, a series of corrections is obtained from simulation that allows alignment between the reconstructed-level energies and masses and the generated-level ones; they ensure that the jet energy scale (JES) or the jet mass scale (JMS) of reconstructed jets is correct (a more precise definition is given below). They also compensate for the effect of multiple proton–proton interactions happening in the same bunch crossing and residual effects in the detector from collisions in nearby crossings (these effects are collectively referred to as *pile-up*). Secondly, other corrections obtained from real data, using known physical

¹ ATLAS uses a right-handed coordinate system with its origin at the nominal interaction point (IP) in the centre of the detector and the z -axis along the beam pipe. The x -axis points from the IP to the centre of the LHC ring, and the y -axis points upwards. Cylindrical coordinates (r, ϕ) are used in the transverse plane, ϕ being the azimuthal angle around the z -axis. The pseudorapidity is defined in terms of the polar angle θ as $\eta = -\ln \tan(\theta/2)$. Angular distance is measured in units of $\Delta R \equiv \sqrt{(\Delta\eta)^2 + (\Delta\phi)^2}$.

processes or well-reconstructed objects such as photons, allow corrections for residual differences (of the order of 2%–3%) to be made between real and simulated reconstructed jets. The calibration method presented in this paper is an alternative simulation-based correction.

Simulation-based corrections are derived from studies of the *individual response* of the quantity of interest E , the jet energy, (but all the following equations stand identically for the mass m), defined by $r_E = \frac{E_{\text{reco}}}{E_{\text{true}}}$ where E_{true} is calculated from the jets clustered from generated particles and E_{reco} , from the jets reconstructed after detector simulation (true and reco jets are more precisely defined in section 4.2). Because of the stochastic nature of both the quantum chromodynamics (QCD) shower and its interactions with the detector, true jets that have the same parameters (such as energy, angular position, mass, ...) can generate distributions of possible r_E . Individual response distributions depend on these parameters and are usually unimodal: their most probable value, their mode $R_E = \text{mode}(\{r_E\})$, is called the *average response*, JES (or JMS in the equivalent case for jet mass), or simply *response* when the context is non-ambiguous. The mode, as opposed to the mean or the median, is chosen as the definition of such a central value to avoid ambiguities or biases that can arise when the distributions are asymmetric. The width of the distribution around the mode is used to define the resolution in E . In this paper, the chosen definition is the inter quantile range (IQR) at 68%² divided by the mode $\sigma_E = \frac{\text{IQR}_{68\%}(\{r_E\})}{R_E}$. Because of experimental limitations, the average response may differ from unity and the objective of the calibration is to find the relevant corrections such that $R_E = 1$ for all populations of true jets (which formalises the idea that true and reco scales are *on average* identical), with σ_E as small as possible.

The individual response distributions can be parameterised by a set of parameters describing the true jet (here taken to be the energy, pseudorapidity and mass) but also by inter-dependent parameters of the reconstructed jets such as the energy, pseudorapidity, mass, fractions of energy deposited in the various layers of the calorimeter, fraction of the momentum of the associated tracks, and others. Formally, it is then possible to model the distribution as a probability distribution function $P(r_E | \vec{x})$ where \vec{x} is the list of input parameters that can be separated into the various true and reconstructed parameters $\vec{x} = (\vec{x}_{\text{true}}, \vec{x}_{\text{reco}})$. The average response for true jets with parameters \vec{x}_{true} is then given by

$$R_E(\vec{x}_{\text{true}}) = \text{mode}(P(r_E | \vec{x}_{\text{true}})). \quad (1)$$

The aim of the calibration is then to find a function of the reconstructed parameters $C(\vec{x}_{\text{reco}})$ defining the calibrated quantity $E_{\text{calib}} = C(\vec{x}_{\text{reco}})E_{\text{reco}}$ such that the most probable value becomes

$$R_{E_{\text{calib}}}(\vec{x}_{\text{true}}) = \text{mode}(P(r_E \times C(\vec{x}_{\text{reco}}) | \vec{x}_{\text{true}})) = 1$$

where $P(r_E \times C(\vec{x}_{\text{reco}}))$ is the probability distribution function obtained from $P(r_E)$ by changing $r_E \rightarrow r_{E_{\text{calib}}} = r_E \times C(\vec{x}_{\text{reco}})$ and the mode is taken over all \vec{x}_{reco} .

In general this mathematical problem is difficult. It has an exact solution in simple cases where the response depends on only one parameter, the quantity E itself, and when $R_E(E_{\text{true}})E_{\text{true}}$ is an affine function [13]. In this case the solution is to choose the function C such as

$$\forall x \in \mathbb{R}, \quad C(xR_E(x)) = \frac{1}{R_E(x)}. \quad (2)$$

This solution is called the *numerical inversion* (NI) because R_E (and thus the pair $(xR_E(x), \frac{1}{R_E(x)})$) can be obtained *numerically* from the simulated data and because $E_{\text{true}}R_E(E_{\text{true}})$ represents an *inversion* of the true quantity³. This method (referred to here as *standard calibration*) is employed by ATLAS to obtain sequentially a jet energy scale calibration and then a mass scale calibration. In practice, in the standard calibration, R_E is evaluated as a function of $(E_{\text{true}}, \eta_{\text{true}})$ (and m_{true} for mass calibration) by collecting individual responses in bins of these quantities. This function R_E is then converted into a correction factor function depending only on reconstructed quantities $(E_{\text{reco}}, \eta_{\text{reco}}$ and $m_{\text{reco}})$ according to the NI principles described above and further detailed in [2, 14]. This procedure gives satisfactory performance. The variables E , η and m are the principal dependencies of the JES and JMS and the use of true quantities to form the response evaluation bins allows potential biases due to the energy or mass spectrum of the generated sample to be avoided when evaluating the average response.

As mentioned above, there is much more information available to describe the reconstructed hadronic showers than just the energy, pseudorapidity and mass. Using these additional variables can potentially help

² IQR instead of the standard deviation is chosen here as the shape of the response distribution does not always follow a Gaussian distribution, particularly for the jet mass.

³ For a given E_{true} , the most probable E_{reco} is by definition $E_{\text{true}}R_E(E_{\text{true}})$.

obtain a more precise JES and JMS and improve their resolution, including subsamples of jets such as quark-initiated or gluon-initiated jets. However, these variables can be correlated. Optimally exploiting all the correlations in the same way as performed in the standard calibration would require highly multidimensional bins, which is practically impossible. On the other hand the task of numerically modelling a multidimensional function can be successfully performed with modern DNN techniques. Furthermore, a key problem of the calibration evaluation, estimating the mode of distributions, is solvable with these techniques; a solution is discussed in detail in section 5.1. A proof of concept of using DNN for JES and JMS calibration, including an implementation of the NI procedure, has already been presented in [15] and DNN techniques are also employed to perform a particular step of the energy (but not the mass) calibration for small- R jets [16]. Building on this, a complete and operational solution and its performance is presented here. This new procedure extends several aspects of the DNN calibration but does not implement NI to simplify the method by avoiding the need to train two DNNs sequentially, one to model the function R as a function of x_{true} , the second the function C as in equation (2). Instead, it evaluates directly the uncalibrated responses in terms of reconstructed quantities, which means that the network evaluates

$$R_E(\vec{x}_{\text{reco}}) = \text{mode}(P(r_E | \vec{x}_{\text{reco}})) \quad (3)$$

instead of $\text{mode}(P(r_E | \vec{x}_{\text{true}}))$ as in equation (1). The calibration function is then chosen to be simply $1/R_E(\vec{x}_{\text{reco}})$. The price to pay for this simpler procedure is that the response $\text{mode}(P(r_E | \vec{x}_{\text{reco}}))$ *a priori* depends on the distribution of the simulated input samples and this dependency can bias the resulting calibration even in the simple cases where the standard calibration, which uses $\text{mode}(P(r_E | \vec{x}_{\text{true}}))$, would not be biased. However, because \vec{x}_{reco} includes many variables relevant to the description of the hadronic shower, it can be expected that the response distributions at each point of the phase space are narrow enough so that the overall bias on the mode is negligible. Although this hypothesis is not testable in practice because of the high dimensionality, verifications are performed to ensure the input samples do not bias the performance (they are presented in section 6.3.1).

4. Samples and selections

4.1. Event simulation

The training and validation of the DNN is based on Monte Carlo simulations of proton–proton (pp) collisions at a centre-of-mass energy of $\sqrt{s} = 13$ TeV. All events were passed through the complete ATLAS detector simulation based on GEANT4 [17, 18]. Various physics processes were simulated as described in table 1 to train and test the DNN on different jet topologies.

Training is performed on the QCD dijet sample as this type of process is, by orders of magnitude, more probable at the LHC and enters as a background to many analyses. In a validation step, it is verified that the training generalises and produces a good calibration for other important physics processes such as those listed in table 1. All samples (except the SHERPA one) were produced using PYTHIA 8.230 [19] with the NNPDF2.3LO [20] parton distribution function (PDF) set and the A14 set of tuned parameters [21]. The training sample containing jets originating from light quarks or gluons was obtained by generating dijets in slices of the jet transverse momentum, p_T , to sufficiently populate the kinematic region of interest (from around 200 GeV up to 6000 GeV). For the validation samples, physics processes modelling phenomena beyond the Standard Model are used to populate the high- p_T region.

- The W/Z -boson sample was obtained by generating the $W' \rightarrow WZ \rightarrow qq\bar{q}\bar{q}$ process with $m_{W'} = 2$ TeV.
- The top-quark sample was obtained by generating the $Z' \rightarrow t\bar{t} \rightarrow W^+b W^- \bar{b} \rightarrow bq\bar{q} \bar{b}q\bar{q}$ process with $m_{Z'} = 4$ TeV.
- The sample of Higgs bosons, which displays a broad Higgs boson p_T spectrum, was obtained by generating the production of Randall–Sundrum gravitons G^* in a benchmark model with a warped extra dimension [22] over a range of graviton masses from 300 to 6000 GeV, where the graviton decays according to $G^* \rightarrow HH \rightarrow b\bar{b}b\bar{b}$.

The SHERPA dijet sample was generated using the SHERPA 2.2.5 [23] generator. The matrix element calculation was included for the $2 \rightarrow 2$ process at leading order, and the default SHERPA parton shower [24] based on Catani–Seymour dipole factorisation was used for the showering with p_T ordering, using the CT14NNLO PDF set [25]. These samples used the dedicated SHERPA AHADIC model for hadronisation [26], based on cluster fragmentation ideas.

Finally, the effect of multiple interactions in the same and neighbouring bunch crossings (*pile-up*) was modelled by overlaying the simulated hard-scattering event (event of interest) with inelastic pp events

Table 1. Simulated samples used for training and validation.

Use	Process type	Generator	Number of jets passing the selections (in millions)
Training, validation	QCD dijet	PYTHIA 8.230	~270
Validation	W/Z	PYTHIA 8.230	~20
Validation	Top quark	PYTHIA 8.230	~15
Validation	Higgs Boson	PYTHIA 8.230	~15
Validation	QCD dijet	SHERPA 2.2.5	~30

generated with PYTHIA 8.186 [27] using the NNPDF2.3LO set of PDFs [20] and the A3 set of tuned parameters [28]. The number of overlaid events is representative of the amount of pile-up present in the 2017–2018 ATLAS pp data sample.

4.2. Jet reconstruction and selection

In each event, the flow of hadronic particles is represented by a set of 4-vectors built by combining momentum and energy measurements from the inner tracker and calorimeters. In this paper, the combination technique producing *unified flow objects* (UFO) [29] is used. These input constituents are clustered into jets with the anti- k_t jet algorithm with angular radius $R = 1.0$ [30] using the FASTJET software package [31]. The jets then undergo a *grooming* procedure aimed at suppressing soft radiation from pile-up and the underlying event; the *soft-drop* procedure [32] is employed with parameters $\beta = 1$ and $z_{\text{cut}} = 0.1$.

Stable particles, with a lifetime $c\tau > 10$ mm, produced by the generators (with the exception of neutrinos and muons) are also clustered into jets using the same algorithm to obtain *true* jets.

To obtain training samples that are not biased by experimental effects such as pile-up, noise or misidentifications, some requirements are imposed on the jets. Reconstructed jets are selected if they are matched to a true jet and isolated as described in [2]. A reconstructed and a true jet are matched if they are within an angular distance $\Delta R = 0.3$. Two isolation requirements are then applied; reconstructed jets are rejected if a true jet other than the matched one is found within $\Delta R = 2.5$ or if another reconstructed jet is found within $\Delta R = 1.5$. Finally, both the reconstructed and true jets are required to have $p_T > 50$ GeV and, in an event, only the two highest- p_T jets satisfying these criteria are considered. The selection results in about 270 million jets being available for the DNN training sample.

5. Methodology of the deep neural network calibration

The simultaneous calibration of the jet energy and mass is performed using the calculations of a single DNN taking as inputs reconstructed jet-level and event-level quantities. The DNN is set up to output two numbers corresponding to the energy and mass responses. However, as mentioned in the previous section, it is not possible to directly predict the exact individual E (or m) response for a given reconstructed jet as each true jet corresponds to a distribution of possible responses. The DNN predictions are thus interpreted as the most probable values of the possible responses for the input jets (that is, the modes of their distribution). Following equation (3), the DNN is trained so that

$$R_E^{\text{DNN}}(\vec{x}_{\text{reco}}) \simeq R_E(\vec{x}_{\text{reco}}) \equiv \text{mode}(P(r_E | \vec{x}_{\text{reco}})).$$

The calibrated energy (or mass) is then defined as

$$E_{\text{calib}} = \frac{E_{\text{reco}}}{R_E^{\text{DNN}}(\vec{x}_{\text{reco}})}.$$

Thus, the DNN output predictions are

$$\vec{y}_{\text{pred}} = (R_E^{\text{DNN}}, R_m^{\text{DNN}}).$$

During the training, the target quantities corresponding to the inputs \vec{x}_{reco} are the individual responses discussed in section 3:

$$\vec{y}_{\text{target}} = \vec{y}_{\text{true}} = (r_E, r_m) = \left(\frac{E_{\text{reco}}}{E_{\text{true}}}, \frac{m_{\text{reco}}}{m_{\text{true}}} \right).$$

These are not directly the desired *average* responses R_E and R_m and the necessity to predict distribution modes (and not means nor medians) requires a careful choice of the loss function. Beside these mathematical

concerns, experimental difficulties related to the detector geometry—and especially the geometry of the calorimeters—strongly interfere in the calibration predictions for certain angular regions. This is accounted for by a dedicated processing of the jet angular position.

Finally, the mass calibration alone has specific difficulties. Firstly, the mass response distributions are generally wider and asymmetric, making it harder for the DNN to predict their mode. Secondly, large- R jets are mainly used to reconstruct heavy particles whose decays are collimated (top quarks, W , Z , or Higgs bosons) and for which the mass measurement is crucial. So the DNN performance needs to be good for these jets, even if their topology differs from standard QCD jets. This has motivated the use of a specific architecture (including a *residual connection*-like structure) and training procedure (with a dedicated mass-only step).

5.1. Loss function

The loss function $\mathcal{L}(\vec{y}_{\text{true}}, \vec{y}_{\text{pred}})$ is a crucial part of the DNN training as it defines what mathematical quantity the DNN will learn to predict. This is particularly true in the case presented here where the targets (\vec{y}_{true}) are realisations of a stochastic distribution. In this case, it is proven that minimising the usual mean square error loss ($\mathcal{L} = (\vec{y}_{\text{true}} - \vec{y}_{\text{pred}})^2$) would have \vec{y}_{pred} converge to the mean of the distribution, while minimising the mean absolute error ($\mathcal{L} = |\vec{y}_{\text{true}} - \vec{y}_{\text{pred}}|$) would imply a convergence to the median [33]. Converging to the distribution mode, as is necessary for the jet calibration, would require taking a Dirac delta distribution as the loss $\mathcal{L} = \delta(\vec{y}_{\text{true}} - \vec{y}_{\text{pred}})$. This is not possible in practice and an approximate function is therefore necessary. One possibility is the Gaussian kernel as suggested in [33], another solution is inspired by mixture-density-network (MDN) techniques and is described below. Numerical tests show the MDN losses are less biased than the Gaussian kernel losses. They are also found to converge faster and allow more flexibility in the training procedure.

First, as the DNN produces two outputs $\vec{y}_{\text{pred}} = (R_E^{\text{DNN}}, R_m^{\text{DNN}})$, two independent loss functions are considered, the sum of them being the final minimised quantity:

$$\mathcal{L}_{\text{tot}} = \mathcal{L}_E + \mathcal{L}_m.$$

The MDN loss is constructed from the assumption that the response distribution of the DNN targets is a Gaussian distribution with central value μ and width σ

$$P(r_E, (\mu, \sigma)) \propto \frac{e^{-(r_E - \mu)^2 / 2\sigma^2}}{\sigma}.$$

With the parameter of interest being μ (the mode of the distribution), an estimator $\hat{\mu}$ (and $\hat{\sigma}$) can be obtained from the maximum of the likelihood (LH) over a given sample of r_E

$$\text{LH}(\mu, \sigma) = \prod_{r_E} P(r_E, (\mu, \sigma)). \quad (4)$$

As a consequence, a DNN outputting two values $\vec{y}_{\text{pred}} = (\mu_{\text{pred}}, \sigma_{\text{pred}})$ and trained with the loss:

$$\mathcal{L}_{\text{MDN}} = -\log(P(\vec{y}_{\text{true}}, \vec{y}_{\text{pred}})) = \log(\sigma_{\text{pred}}) + \frac{1}{2} \frac{(r_E - \mu_{\text{pred}})^2}{\sigma_{\text{pred}}^2} \quad (5)$$

would minimise the logarithm of equation (4) and thus predict the estimators, that is $(\mu_{\text{pred}}, \sigma_{\text{pred}}) = (\hat{\mu}, \hat{\sigma})$. Using this MDN loss, the DNN has to predict the width of this distribution (σ_{pred}) in addition to predicting the mode of the response distribution. For an energy and mass calibration DNN:

$$\vec{y}_{\text{pred}} = \begin{pmatrix} \mu_{\text{pred}}^E \\ \sigma_{\text{pred}}^E \\ \mu_{\text{pred}}^m \\ \sigma_{\text{pred}}^m \end{pmatrix},$$

where only the predicted modes are eventually used in the final calibration procedures.

Table 2. The input features of the DNN.

	Name	Definition
Jet level	E	Energy of the jet in GeV, $\log E$ is taken to reduce the spread of its distribution
	m	Mass of the jet in GeV, $\log m$ is taken to reduce the spread of its distribution
	η	Jet pseudorapidity
Substructure level	groomMRatio	Mass ratio of groomed to ungroomed jets
	Width	$\sum_i p_{Ti} \Delta R(i, \text{jet}) / (\sum_i p_{Ti})$ where ΔR is the angular distance (sum over the jet constituents)
	Split12, Split23	Splitting scales at the 1st and 2nd exclusive k_T declusterings [35]
	C2, D2	Energy correlation ratios [36, 37]
	τ_{21}, τ_{32}	N-Subjettiness ratios using WTA axis [38, 39]
	Qw	Smallest invariant mass among the proto-jets pairs of the last 3 steps of a k_T reclustering sequence
Detector level	EMFrac	Energy fraction deposited in the electromagnetic calorimeter
	EM3Frac	Energy fraction deposited in the third layer of the electromagnetic calorimeter
	Tile0Frac	Energy fraction deposited in the 1st layer of the hadronic calorimeter
	EffNConsts	$(\sum_i E_i)^2 / (\sum_i E_i^2)$ (sum over the jet constituents)
	NeutralFrac	Energy fraction from neutral constituents
	ChargedPTFrac	p_T fraction from charged constituents
	ChargedMFrac	Mass fraction from charged constituents
Event level	μ	Mean number of interactions per bunch crossing
	NPV	Number of primary vertices per event

In practice, the energy or mass response distributions are not perfect Gaussian distributions especially for jets with low p_T and high mass or with high $|\eta|$. To take this into account, the assumed underlying distribution can be replaced by an asymmetric Gaussian distribution or a truncated Gaussian distribution.

$$P_{\text{asym}}(x) \sim \begin{cases} e^{(x-\mu)^2/2\sigma_1^2} & \text{if } x < \mu \\ e^{(x-\mu)^2/2\sigma_2^2} & \text{if } x \geq \mu \end{cases} \quad P_{\text{trunc}}(x) \sim \begin{cases} e^{(x-\mu)^2/2\sigma^2} & \text{if } |x-\mu| < N\sigma \\ 0 & \text{otherwise.} \end{cases} \quad (6)$$

Although not physically motivated these losses help with the numerical convergence of the network. In particular, the asymmetric MDN loss (MDNA) helps to avoid biases from asymmetric shapes in the response distributions, but it requires the DNN to output three values per prediction $(\mu, \sigma_1, \sigma_2)$. The use of a truncated distribution can apply to both the MDN and MDNA cases. In practice, truncation consists of excluding from the loss evaluation jets for which $|x - \mu| > N\sigma$ and adapting equation (5) with the relevant distribution normalisation factor. Asymmetric loss helps to converge faster in regions of phase space where the distributions are asymmetric and the truncation is used at the end of the training to improve the accuracy of the calibration. Details of the choice and tuning of the parameters of the loss function are further discussed in section 5.4.

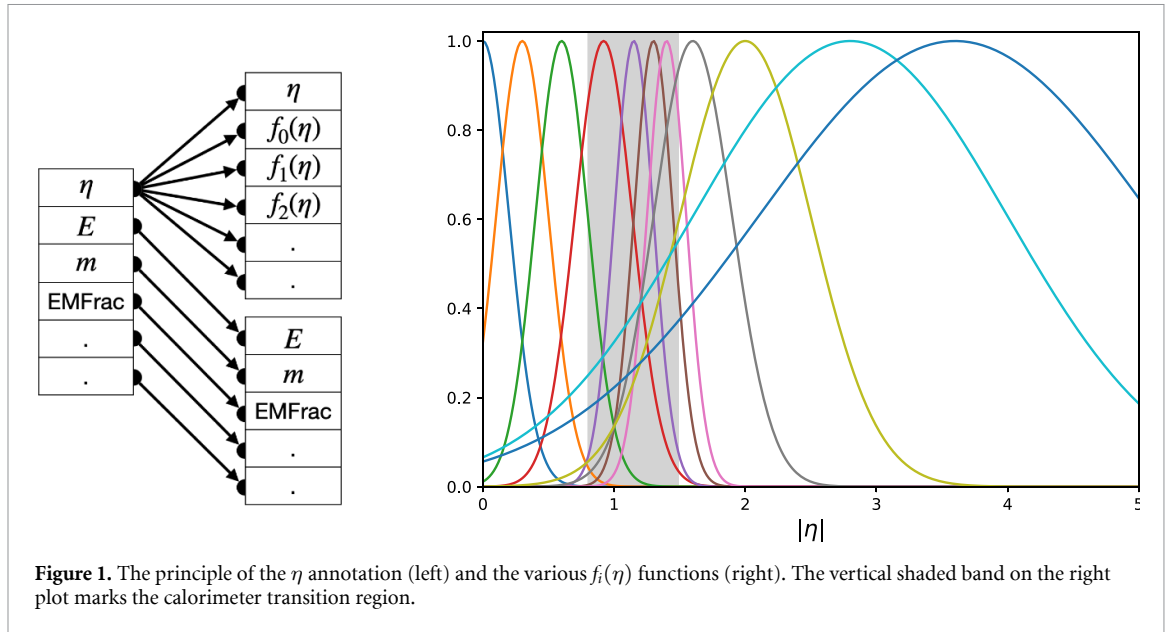
5.2. Input features

To obtain precise predictions, it is necessary to give the DNN an as complete description of the jet and the event as possible. A list of 21 jet or event variables is chosen as the input to the DNN. These features are chosen for their relevance in calibration or jet identification tasks as demonstrated in previous studies [2, 34]. They can be divided in four categories: the jet kinematics, which are the main dependencies of the energy and mass responses⁴; the jet substructure variables, which describe the particle-shower topology used to classify jets; the detector variables, which quantify the relative charged-particle contribution and the development of the calorimeter showers; and finally, the event variables that describe the jet environment. Table 2 presents these input variables and their definitions. To have homogeneous inputs for the DNN, each input is normalised so that its distribution falls in the range of $[-1, 1]$.

In addition, the DNN has difficulties learning the sharp variations in the energy and mass responses along η that are due to the complex ATLAS detector geometry and in particular to the poorly instrumented regions between the central and forward calorimeters between $|\eta| = 0.8$ and $|\eta| = 1.5$.

In an effort to help the modelling, an additional input preparation step called η annotation is implemented as the first operation of the DNN. This step computes extra features based on η that are passed

⁴ Although the rapidity provides a better estimate of the actual angular position of massive objects, the pseudorapidity is used in this paper as used in the current ATLAS calibration; the performance is not expected to be affected by this choice.



along with other input features to the rest of the DNN. These extra features are calculated as $f_i(\eta)$ where f_i are Gaussian functions with different central values and widths that are chosen to cover key angular regions of the detector (such as the central part or edges of the electromagnetic barrel calorimeter and of other calorimeters). Figure 1 shows how the 11 different Gaussian functions are positioned, providing a continuous encoding of the proximity of the jet to these regions. These processed values are included alongside the unprocessed η for a total of 12 representations.

5.3. Architecture

The DNN architecture is mainly based on two specific parts, the η annotation (described in section 5.2) and a fork between the energy and mass outputs. Both are designed to address the main difficulties of the jet calibration, the η dependency of the responses and the important differences between the energy and mass response distributions. Building on this base, the architecture was iteratively improved and tested to obtain a structure giving good performance. Consequently, the DNN has a relatively complex structure as represented in figure 2, where:

- *Dense* (N) blocks represent the matrix, bias and activation function resulting in a hidden layer with N neurons.
- The *Concatenate* block is a static layer (without trainable parameters) that concatenates its two input layers.
- The *Multiply* block is a static layer that performs an element-wise multiplication of its input layers.
- The final *Output* layers give the predictions for the energy and mass responses. They may consist of two or three neurons depending on the loss function (as discussed in section 5.1).

The DNN contains approximately 764 000 trainable parameters and is structured in different parts as indicated in figure 2:

- **Input processing:** contains the input layer with the 21 input features and the η annotation described above.
- **Core:** contains several hidden layers (210 neurons each) common to both the energy and mass predictions.
- **Early fork:** premature splitting between the energy and mass predictions to allow for a strong specialisation of the DNN in each calibration, both forks containing the same hidden layers. Having independent weights also allows to *freeze* some of them during the training procedure.
- **Multiplicative residual connection:** loosely inspired from [40] with the substitution of the addition by a multiplication to increase the class of functions that can be modelled by the network. These layers link the input layer directly to the mass output, with the intention of making the DNN learn which inputs are the most important for the mass calibration and thus helping to improve the mass predictions⁵.

⁵ This is only added for the mass calibration prediction as it is harder to predict than the energy calibration due to its response distributions being broader and more asymmetric. The predicted energy calibration already shows excellent performance without an additional residual connection.

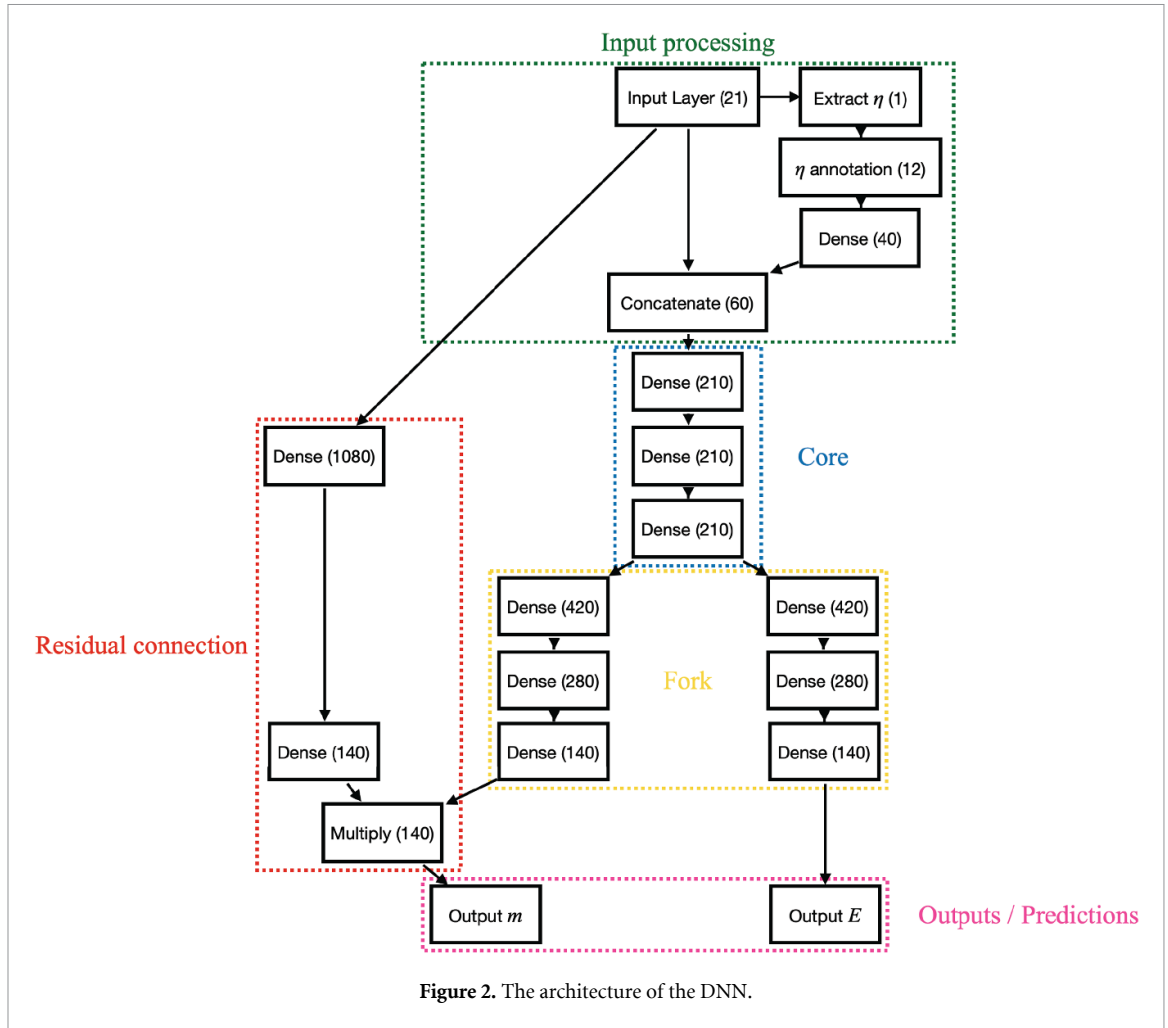


Figure 2. The architecture of the DNN.

- Outputs: the DNN has two output predictions, one for the energy calibration and one for the mass calibration, $\vec{y}_{\text{pred}} = (\mu_{\text{pred}}^E, \mu_{\text{pred}}^m) = (R_E^{\text{DNN}}, R_m^{\text{DNN}})$, along with subsidiary predictions $(\sigma_{\text{pred}}^E, \sigma_{\text{pred}}^m)$.

The activation function for each hidden layer is chosen to be the MISH function [41] and is given by:

$$f(x) = x \tanh(\ln(1 + e^x)).$$

The only exception is the activation function of the last hidden layer of the residual connection that is the *softmax* function: its outputs are restricted to $[0, 1]$ and are used as multiplicative weights.

The last activation function applied to the output layers is chosen to be:

$$f(x) = \tanh(x) + 1$$

to obtain predictions between 0 and 2, which is the expected range of the energy and mass central responses.

5.4. Training procedure

Establishing the training strategy cannot be left to a simple hyperparameter scan. Firstly, because the energy and mass responses vary significantly across the phase space that is not uniformly populated and, secondly, because converging to a loss minimum does not guarantee that the physics performance goals are satisfied for the full phase space. Furthermore, these performance goals (described in section 6) are costly to evaluate and cannot be tested during the training procedure. As a consequence the strategy presented here is obtained with a series of attempts and refinements gradually improving the performance. This training strategy is described in table 3: it totals 107 epochs and is divided into three parts.

In a first initialisation step, the DNN is trained with small batch sizes and an MDNA loss with no or small truncation of the loss. This aims at quickly converging to a rough estimate of the mode of the response distributions thanks to small batch size (i.e. frequent weight updates) and a few epochs while adapting to possible asymmetric distributions (e.g. at high η) with the MDNA loss.

Table 3. The specific training procedure of the DNN. MDN(A) stands for mixture density network (asymmetric). The loss truncation is indicated in number of standard deviations, σ . When E and m are not mentioned, it means that the energy and mass losses are identical.

Steps	No.	Number of epochs	Batch size	Learning rate	Loss
Initialisation	1	2	15 000	10^{-3}	MDNA
	2	2	25 000	10^{-3}	MDNA
	3	2	35 000	10^{-3}	MDNA truncated (4.0σ)
	4	2	15 000	10^{-3}	MDNA truncated (3.5σ)
Common training	5	6	95 000	10^{-3}	MDNA truncated (3.5σ)
	6	6	95 000	10^{-3}	MDNA truncated (3.5σ)
	7	6	125 000	10^{-3}	MDNA truncated (3.2σ)
	8	6	125 000	10^{-3}	MDNA truncated (3.2σ)
	9	10	155 000	5×10^{-4}	MDNA truncated (3.0σ)
	10	15	95 000	10^{-5}	MDNA truncated ($E: 3.0\sigma, m: 2.0\sigma$)
Exclusive mass training	11	50	95 000	10^{-5}	MDN truncated (1.0σ)

The second step is designed to obtain very precise predictions by taking advantage of large batch sizes and a progressive narrowing of the loss truncation. This narrowing allows a gradual focus on the centre of the response distributions, improving the predictions. The larger batch sizes improve the calculation speed and thus the training time.

The third step is a fine-tuning step with an exclusive mass training. The weights involved in the energy prediction⁶ are frozen to their values at the end of the second step and only those involved in the mass prediction⁷ are free to be tuned. This step is necessary in order to have as good predictions for the mass as for the energy for which the two first steps are enough. For this last step, a MDN loss with a large truncation at 1.0σ is used in order to focus more on the core of the mass response distribution. A symmetric loss at this stage is observed to converge better, possibly because it results in a simpler network, easier to optimise on the central and more symmetric parts of the response distributions.

During the training two different optimisers are used, *Rectified Adam* [42] in the initialisation step and *diffGrad* [43] in the common training and exclusive mass training. The learning rate is decreased in the latter steps of the training following the improvements in the predictions.

6. Performance and validation of the calibration

The evaluation of the DNN performance and the validation of the predicted energy and mass calibrations are presented in this section. Unless mentioned otherwise, these are evaluated on the dijet sample, hence for standard quark and gluon jets.

6.1. Technical performance

For this study, the validation data sample is a subset of the dijet data sample that is set aside at the beginning of the training (about ten million jets corresponding to $\sim 4\%$ of the training data sample). Figure 3 shows the evolution of the loss with the number of epochs (i.e. the number of jets processed). The training and validation losses (obtained for the energy, the mass and their total) are shown as solid and dotted lines, respectively. The different losses display very good agreement, showing that the DNN does not overfit the training data sample, as expected given the size of the training data sample; overfitting would take many more epochs. It also shows that the loss does not evolve significantly after two thirds of the training. For a more common DNN set-up, it could be wise to stop the training earlier, as it seems—by that metric alone—that its performance is not improving anymore. However, it is observed that the predicted calibrations continue to improve even if the loss does not, which makes it difficult to find an optimum training procedure.

The consistency of the training is also verified by training DNNs that differ only by weight initialisation and ensuring that their losses and calibration performance are identical.

6.2. Calibration performance

The performance of the energy and mass calibrations are quantified using the response $R_{E_{\text{calib}}}$ and the resolution σ of the calibrated distributions, as defined in section 3.

⁶ These comprise the weights involved in the input processing, the core and the energy-dedicated fork of the network architecture.

⁷ These comprise the weights in the mass-dedicated fork and in the residual connection layers of the network architecture.

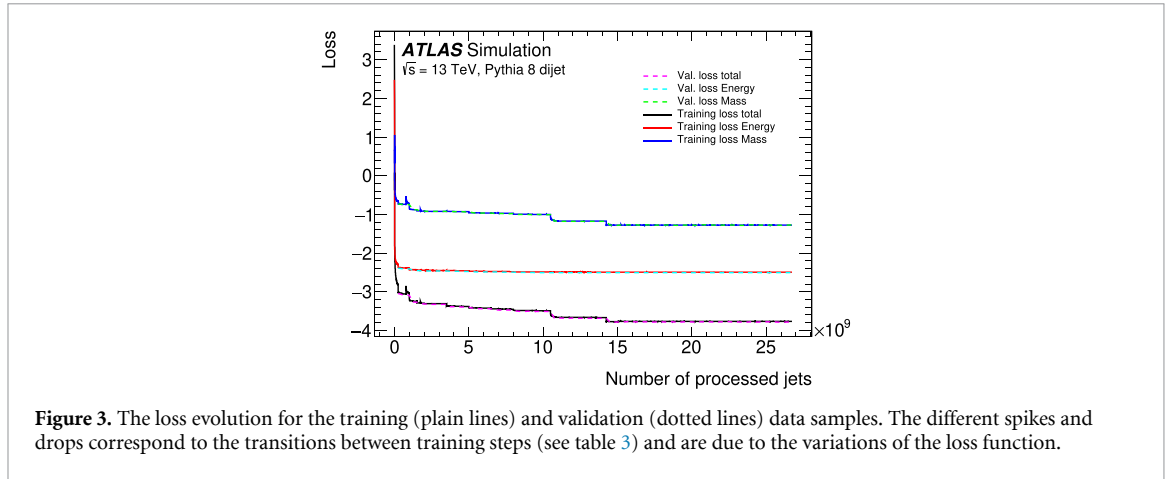


Figure 3. The loss evolution for the training (plain lines) and validation (dotted lines) data samples. The different spikes and drops correspond to the transitions between training steps (see table 3) and are due to the variations of the loss function.

More precisely, from the predicted energy and mass response $\vec{y}_{\text{pred}} = (R_E^{\text{DNN}}, R_m^{\text{DNN}})$, the individual energy (or mass) calibrated response is defined as:

$$r_{E_{\text{calib}}} = \frac{E_{\text{calib}}}{E_{\text{true}}} = \frac{1}{R_E^{\text{DNN}}} \frac{E_{\text{reco}}}{E_{\text{true}}} = \frac{r_E}{R_E^{\text{DNN}}}.$$

As discussed in section 3, $r_{E_{\text{calib}}}$ values are realisations of a distribution P from which the calibrated response can be obtained: $R_{E_{\text{calib}}}(\vec{x}_{\text{true}}) = \text{mode}(P(r_{E_{\text{calib}}} | \vec{x}_{\text{true}}))$. In practice, the individual responses $r_{E_{\text{calib}}}$ are collected in histograms for each bin of x_{true} (where typically $x_{\text{true}} = (p_T^{\text{true}}, m^{\text{true}}, \eta^{\text{true}})$). From these histograms, $R_{E_{\text{calib}}}(x_{\text{true}})$ is extracted from a fit to a Gaussian distribution⁸ and the calibrated response resolution σ from the calculation of the IQR divided by $R_{E_{\text{calib}}}$ (not to be confused with σ_{pred} predicted by the network and described in section 5.1).

In the following, the performance is presented by plotting the response or resolution as a function of one of the bin-defining variables. Better performance is indicated by a response closer to 1.0 (called response closure) and a resolution closer to 0.0 in all of the phase space. All plots include statistical uncertainties computed from the fits of the response distributions but they are generally too small to be visible.

6.2.1. Performance on QCD dijets

As a closure test, the DNN calibration is applied to the QCD sample used during training. This allows verification that the DNN convergence translates into good physics performance in a sample with large statistics. Overall, the calibration is found to perform very well for $|\eta| < 2$ with the best results at high mass in terms of response closure and resolution. Figure 4 presents the energy and mass calibrated responses as a function of p_T^{true} and η^{true} and the energy and mass resolution as a function of p_T^{true} for specific bins. It shows excellent response closure for both energy and mass, closer to unity than the standard calibration [2]. The DNN calibration also shows an important improvement in the resolution relative to the standard calibration. For the mass, the uncalibrated resolution appears better than the calibrated ones. However, this is a relative quantity (as defined in section 3) while the absolute value of the IQR scales with the central value. As a consequence, comparing the uncalibrated resolution corresponding to responses significantly differing from 1.0 with a calibrated resolution is not very meaningful.

Figure 5 presents the excellent consistency of the DNN calibration performance for different p_T^{true} bins.

In every bin of $(p_T^{\text{true}}, m^{\text{true}}, \eta^{\text{true}})$ with $p_T^{\text{true}} > 200$ GeV, $m^{\text{true}} > 40$ GeV and $|\eta^{\text{true}}| < 2$, the DNN calibration is equally or more performant than the standard calibration with a better response closure and resolution. Improvements of a few percent up to around 10% are observed in both energy and mass response closure and resolution.

6.2.2. Effect of η annotation

Section 5.2 describes the necessity to add the η annotation to help the DNN adapt to the complex detector geometry. The assumption is that the extra information represented by the angular encoding together with the related weights allows the training process to specialise the predictions according to the detector region.

⁸ Firstly, the histograms are smoothed with a Savitzky–Golay filter [44] to improve the fit stability in low-statistics bins. Then, heuristics are employed to limit the fit around the central value by setting the fitting range around the mean of the histogram to be between $\pm N\sigma$, where σ is the standard deviation.

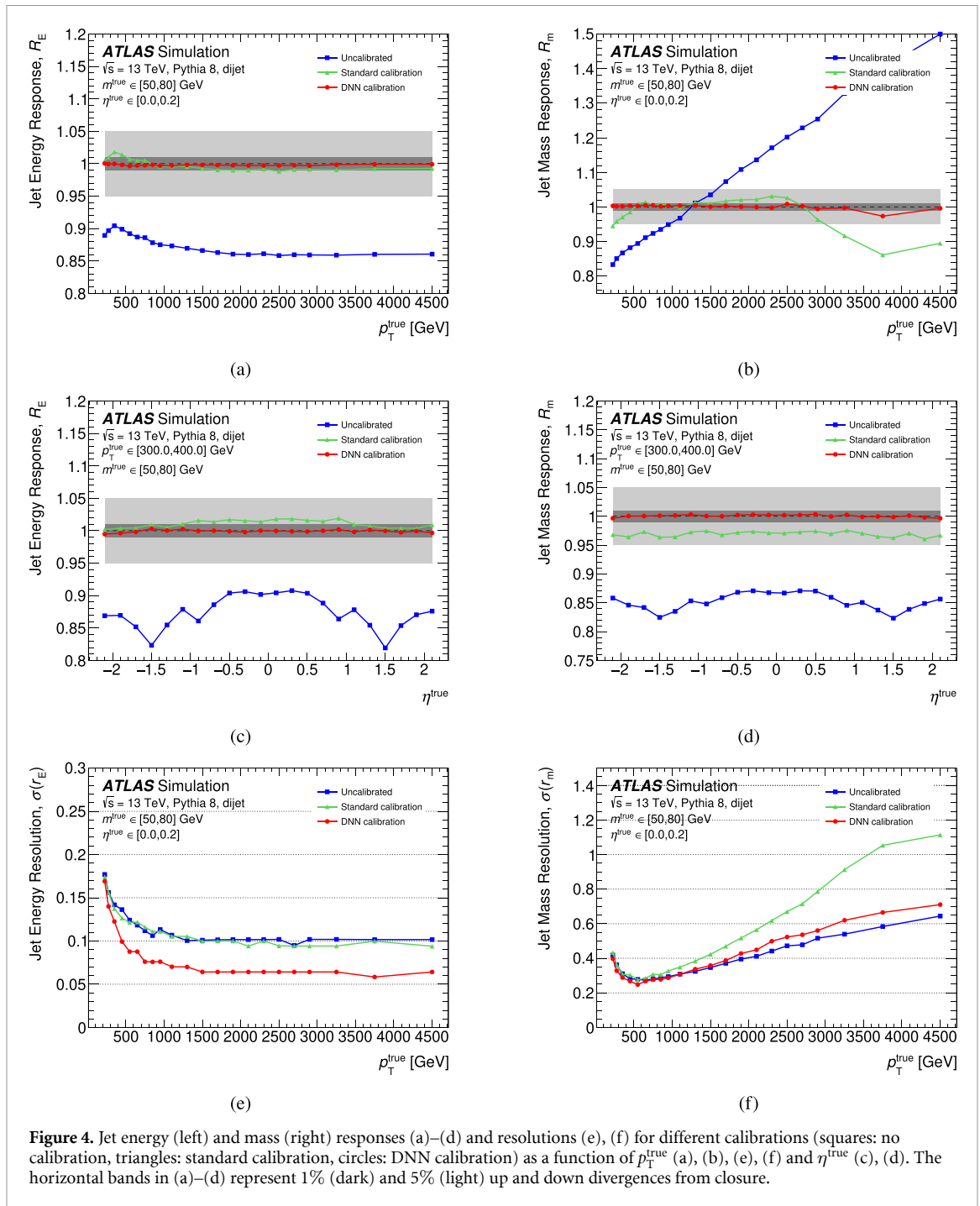


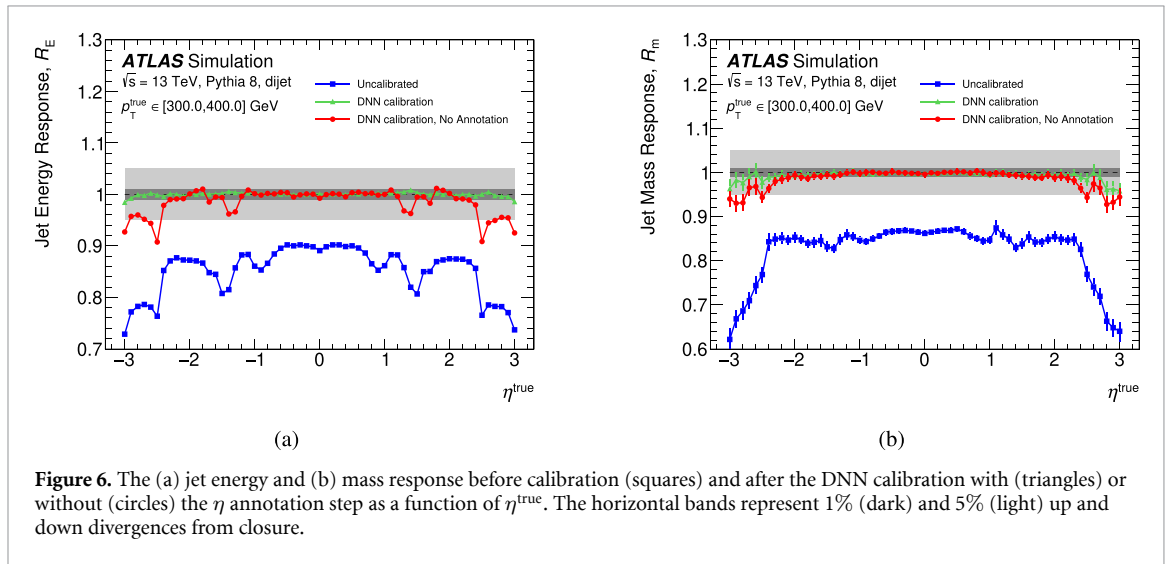
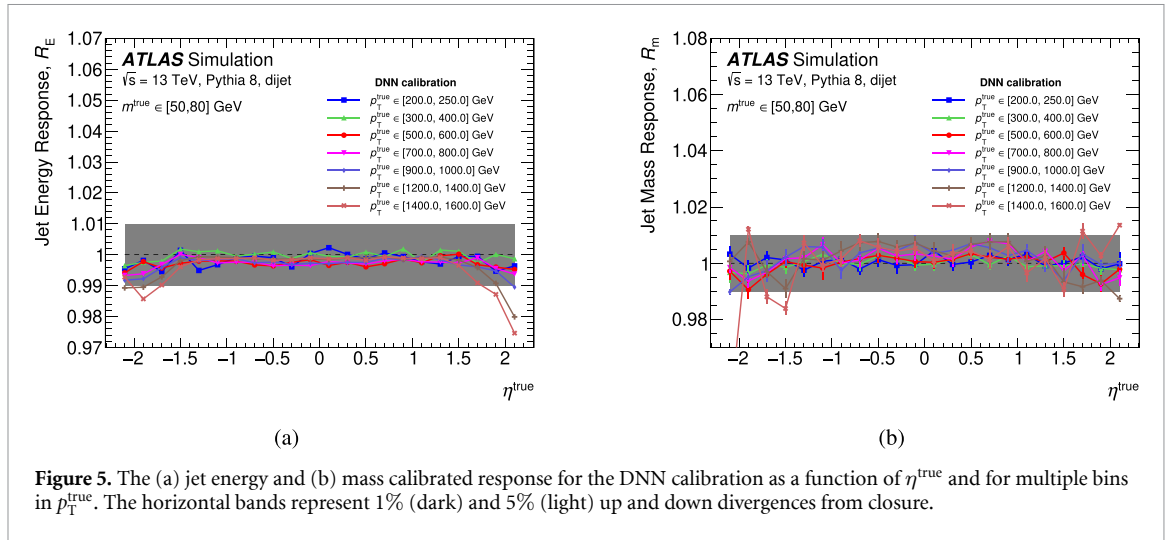
Figure 4. Jet energy (left) and mass (right) responses (a)–(d) and resolutions (e), (f) for different calibrations (squares: no calibration, triangles: standard calibration, circles: DNN calibration) as a function of p_T^{true} (a), (b), (e), (f) and η^{true} (c), (d). The horizontal bands in (a)–(d) represent 1% (dark) and 5% (light) up and down divergences from closure.

As a validation step, figure 6 shows a comparison of the jet energy and mass response closure between two DNN setups with the same training procedure and the same architecture except for the η annotation step. Its inclusion clearly improves the DNN calibrated response closure in the almost complete η range and especially in the calorimeter transition region above $|\eta| = 1.2$. The JMS improvement is less important, as expected since the uncalibrated response (squared markers) variations for the mass are less important than for the energy.

These improvements are present in every p_T and η bin, proving the importance of the η annotation step.

6.2.3. Performance on other topologies

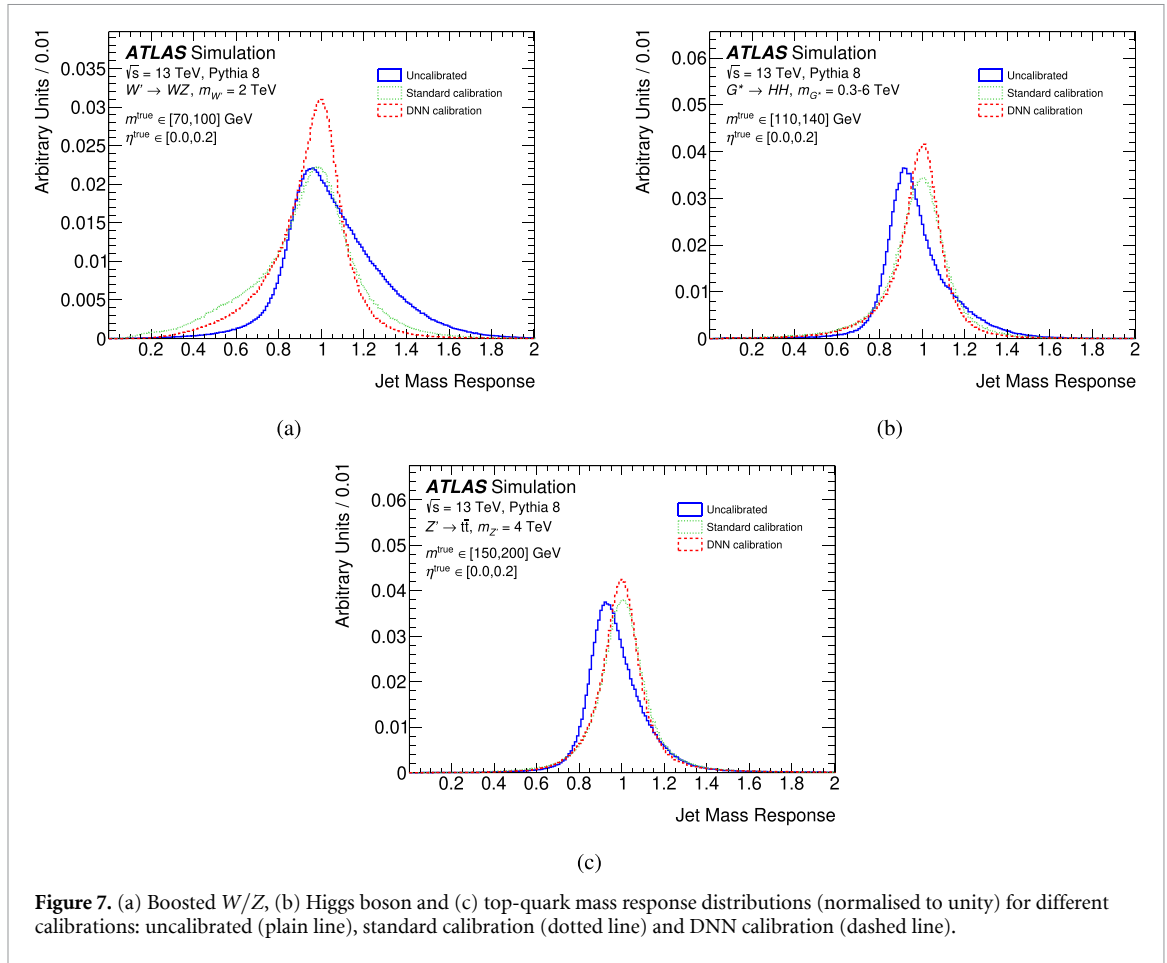
Physics analyses mainly use large- R jets to reconstruct the decays of massive and boosted particles like top quarks, W , Z or Higgs bosons. These decays result in jets with different shower topologies than those originating from the dijet samples with which the DNN is trained; this can have an impact on the mass response as demonstrated in [16] where significant differences between W -initiated and q/g -initiated jets were observed. It is hence very important to verify that the DNN predictions generalise to other such



topologies as the same calibration is applied to all jets in data as their origin will be unknown. For this, simulated samples of processes with heavy hadronically decaying particles, as described in section 4.1, are considered. For each sample, the same jet selection and DNN calibration as for QCD jets are applied and the resulting scale and resolution are evaluated in mass bins centred on the mass of the corresponding massive particle. The population of these massive, high-momentum jets is then expected to be entirely dominated by the hadronic decays of the heavy particles considered so that the effect of the topology can be assessed.

Figure 7 presents the jet mass response distributions obtained with boosted massive jets (W/Z , Higgs boson and top-quark decay) for different calibrations (uncalibrated, standard calibration and DNN calibration). It shows the benefits of the DNN calibration compared with the standard calibration or the absence of a calibration; the distributions are narrower with less asymmetric tails and are better centred on 1.0.

Figure 8 shows the jet energy and mass average responses as a function of the true p_T for the same samples and calibrations. As expected, large differences between the different topologies are observed before calibration, especially in the mass response. While both the standard and the DNN calibrations reduce these response differences, the DNN calibration outperforms the standard one as it gives better closure for each topology, showing that the DNN predictions generalise well to more complex topologies. A small non-closure in the energy response is however observed for all the boosted topologies at low p_T^{true} for the DNN calibration. For the W/Z and Higgs boson jets, this small under-performance can easily be explained by the internal structure of the boosted massive jets; at high momentum, W/Z and Higgs boson large- R jets are usually composed of two sub-jets with an angular separation of $\Delta R \sim \frac{2m}{p_T}$. At low p_T , their angular separation becomes comparable to the large- R jet radius of 1.0, and the structure becomes neither 1-prong nor 2-prong. Such a structure is possibly rare in the dijet training sample or not captured by the input



substructure variables, making it impossible for the DNN to learn to correct for this effect. For top-quark jets, a similar effect could be at play when the 3-prong decay $t \rightarrow Wb \rightarrow qq'b$ is not fully contained within the jet radius, thus leading to atypical jets. To solve this difficulty, a dedicated additional network structure and training can be envisaged and is discussed in section 7.

Figure 9 presents the jet energy and mass resolution for the boosted topologies. Here as well, the DNN calibration shows improved performance relative to the standard calibration. The resolution differences between the topologies here can be explained by the increasing mass bins in which the responses are evaluated; the resolution usually gets better at higher masses.

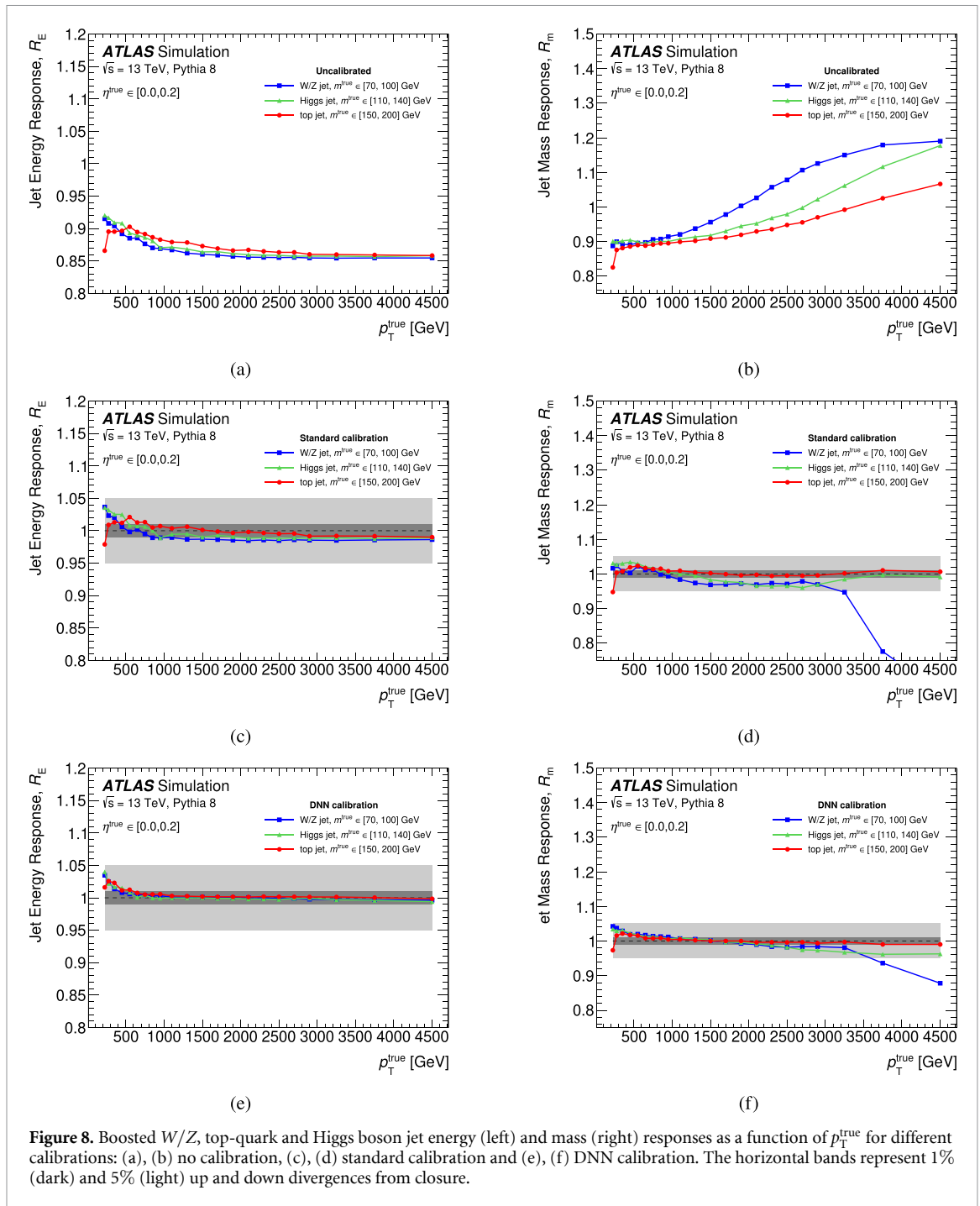
6.3. Validation of the DNN calibration

An extensive series of tests are performed to ensure the good physical behaviour of the DNN calibration. As described above, both the standard and DNN calibrations are tested and compared.

6.3.1. Spectrum dependency

The DNN is trained and validated on a specific set of jets produced through a particular Monte Carlo process with a large range of energy. This set of jets leads to specific distributions of the input variables. The DNN calibration performance should be independent of the distribution to which it is applied, so it can be used in different physics analyses with different event selections resulting in different input distributions. Since the calibration is already assessed as a function of true p_T , the impact of the distribution of this variable (or the energy one) is not expected to be strong. However, other input variables are correlated with the p_T and are not binned in the performance tests; their distribution shapes may thus impact the calibration. To verify this, the performance is re-evaluated by changing the response distributions using statistical weights when constructing the response histograms. The weights are chosen to obtain a flat jet energy distribution, entirely different from the original one used in the training as illustrated in figure 10(a).⁹ The performance is then evaluated in large p_T bins similar to those that physics analysis may use and inside which distribution

⁹ Distributions are shown after transformation and normalisation, e.g. the histogram shows $f(E) = s \times \log(E) + o$ where s and o are such that $f(E)$ is mostly distributed in $[-1, 1]$.



differences may have significant effects. Figures 10(b) and (c) shows the jet energy and mass responses obtained with the DNN calibration with (square markers) and without (triangular markers) re-weighting. The differences between the two calibrated response closures are very small, proving that the DNN calibration does not depend significantly on the input jet distribution.

6.3.2. Pile-up dependency

The impact of the pile-up conditions is tested and evaluated by considering the dependency of the response on two quantifying variables: the number of reconstructed primary vertices in an event, NPV, and the average number of collisions per bunch crossing, μ . For this, the energy (or mass) response $R_{E,\text{calib}}$ is estimated in bins of $(v_{\text{PU}}, E^{\text{true}}, \eta^{\text{true}})$ where v_{PU} is NPV or μ . A linear fit to $R_{E,\text{calib}}$ against v_{PU} is then performed for each $(E^{\text{true}}, \eta^{\text{true}})$ and the corresponding slope, the *gradient* relative to v_{PU} denoted as $\frac{\partial R_E}{\partial v_{\text{PU}}}$, is extracted. Figure 11 presents the gradient relative to NPV of the energy and mass calibrated response modes as a function of η . For both the energy and the mass, the DNN calibration shows smaller gradients than the standard calibration. Similar results are obtained for μ .

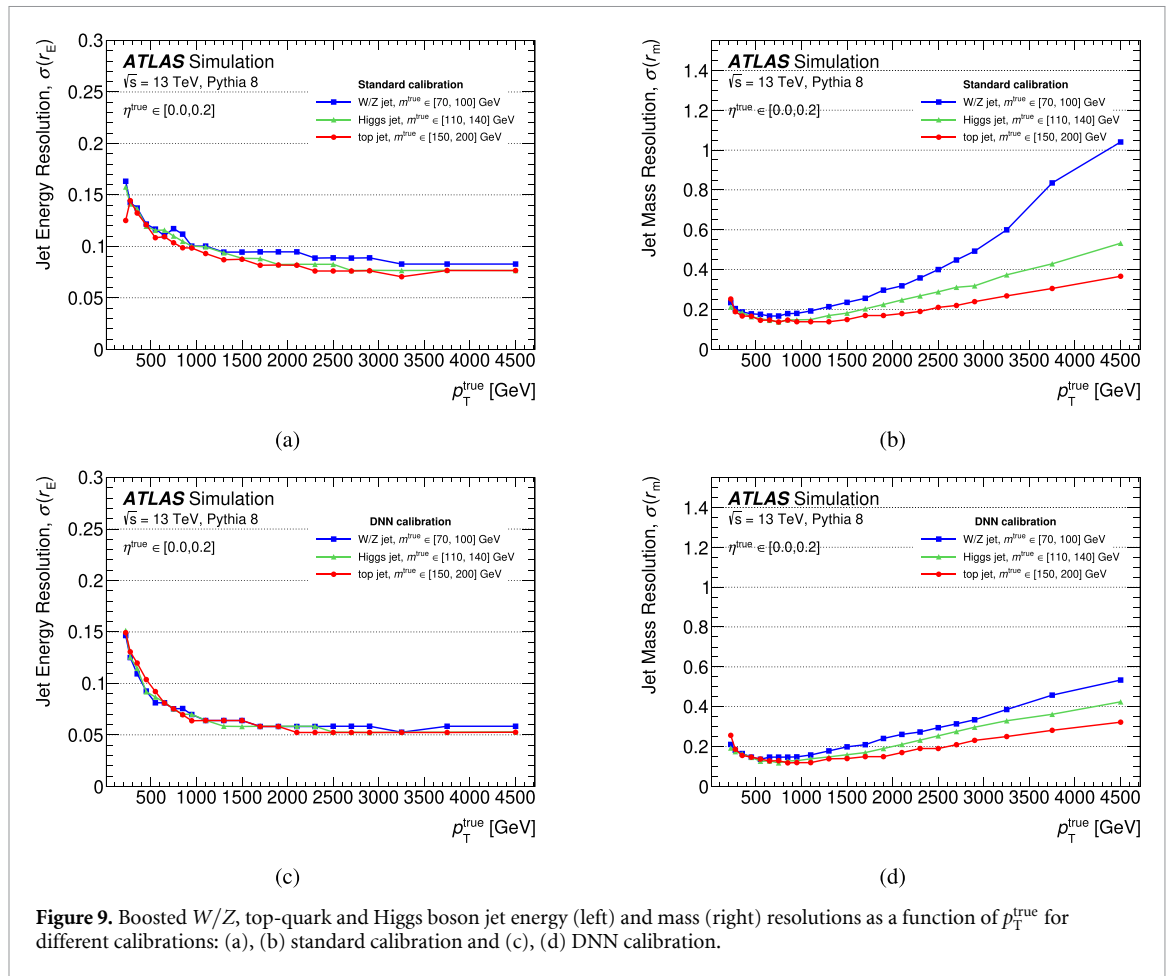


Figure 9. Boosted W/Z, top-quark and Higgs boson jet energy (left) and mass (right) resolutions as a function of p_T^{true} for different calibrations: (a), (b) standard calibration and (c), (d) DNN calibration.

This shows that the grooming procedure performed during the jet reconstruction is not enough to suppress pile-up effects, while the DNN is able to do so by including NPV and μ as input variables.

6.3.3. Jet flavour dependence

As discussed above, the DNN performance is assessed with different topologies (QCD, W/Z, top-quark, or Higgs boson jets). It is also important to understand the dependency of the DNN calibrations on the actual parton that initiated the jet, also known as its flavour (light-quark (u, d, s, c), b -quark or gluon jets), as different responses for different flavours will translate into systematic uncertainties through the uncertainty in the flavour composition of the jets.

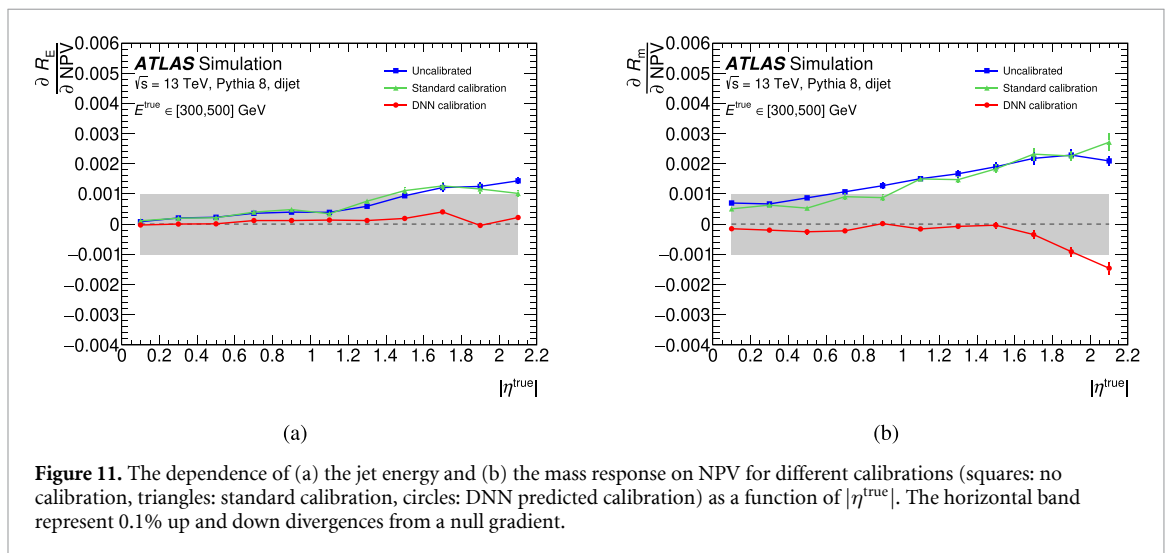
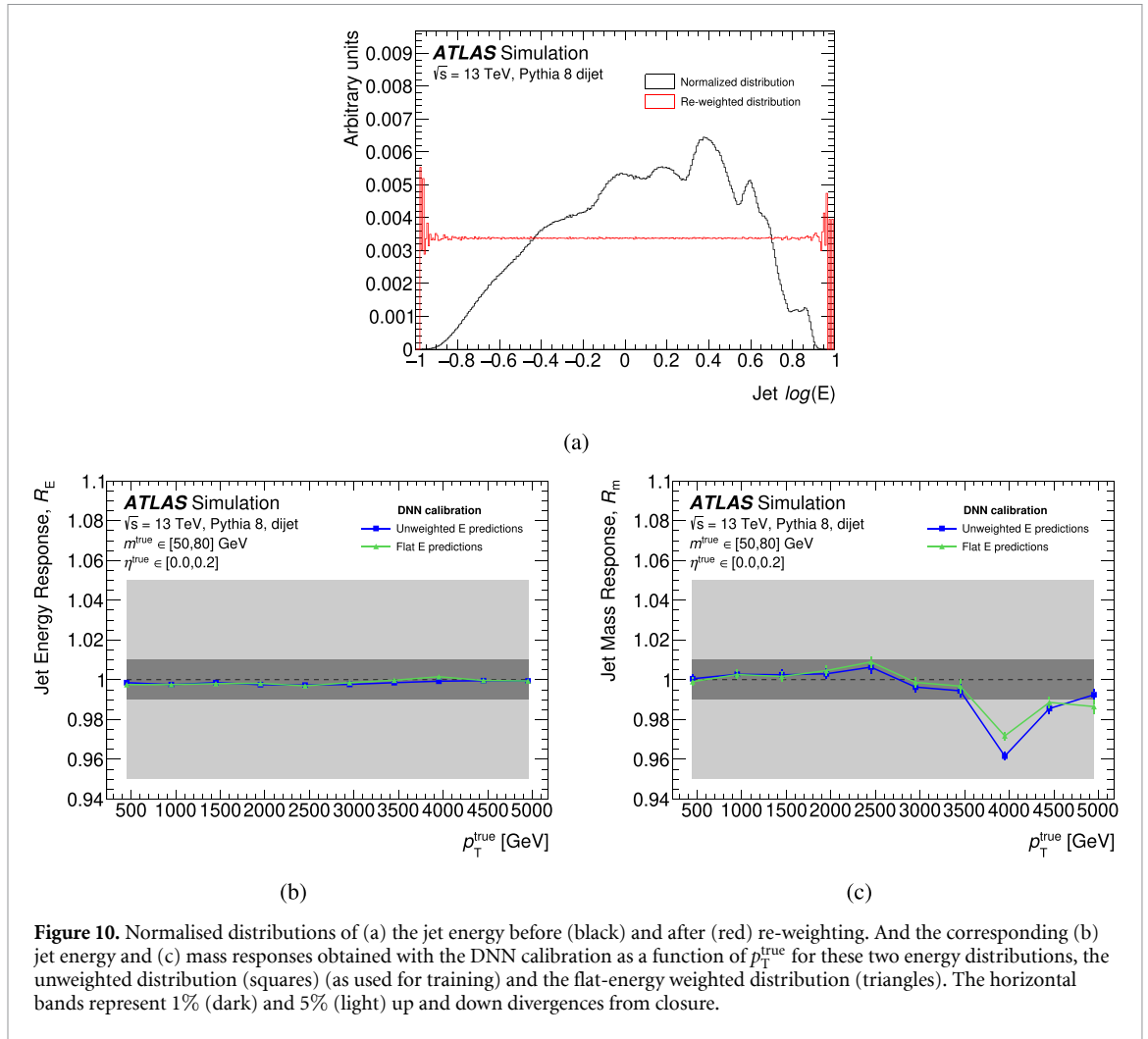
Figure 12 presents the energy and mass calibrated responses as a function of the jet energy for different jet flavours, comparing the DNN calibration to the standard calibration. The jet flavour is defined here as the flavour of the parton with the highest energy in the parton shower. These show that the DNN predicts better calibrations for the different partons, with smaller inter-flavour differences relative to the standard calibration, especially at low p_T .

6.3.4. Dependency on the generator

The DNN calibration will be applied to all simulated samples used in ATLAS analyses that are produced with a variety of generators, as well as jets in real data events. Therefore it is desirable to evaluate if the performance of the network is strongly affected by the modelling of jets within PYTHIA8. Generators have specific ways of evaluating the parton shower and hadronisation resulting in differences in the predicted particle flow and simulated detector showers. Since such differences can be representative of those between simulation and real data, it is important to verify they are not detrimental to the performance of the DNN calibration.

A data sample of SHERPA-generated dijets with the same data preparation as described in section 4.2 is used to compute jet energy and mass responses with the standard calibration and the DNN calibration¹⁰.

¹⁰ The DNN is trained with the PYTHIA sample as discussed in the previous sections.



Both are then compared with the performance obtained with the PYTHIA dijet data sample. Figure 13 shows this comparison. The DNN energy calibration shows almost identical performance for the two generators, except at low p_T^{true} where a small under-performance is observed with the SHERPA data sample although closure is however still obtained. Moreover, the DNN calibration shows a lesser dependency on the generator than the standard calibration for the energy. For the mass calibration with the SHERPA data sample, the DNN response closes within 5% but outside 1% in all the p_T^{true} range. This can be expected as the jet's mass is more dependent on its particle flow structure. This under-performance is observed to be reduced in higher mass

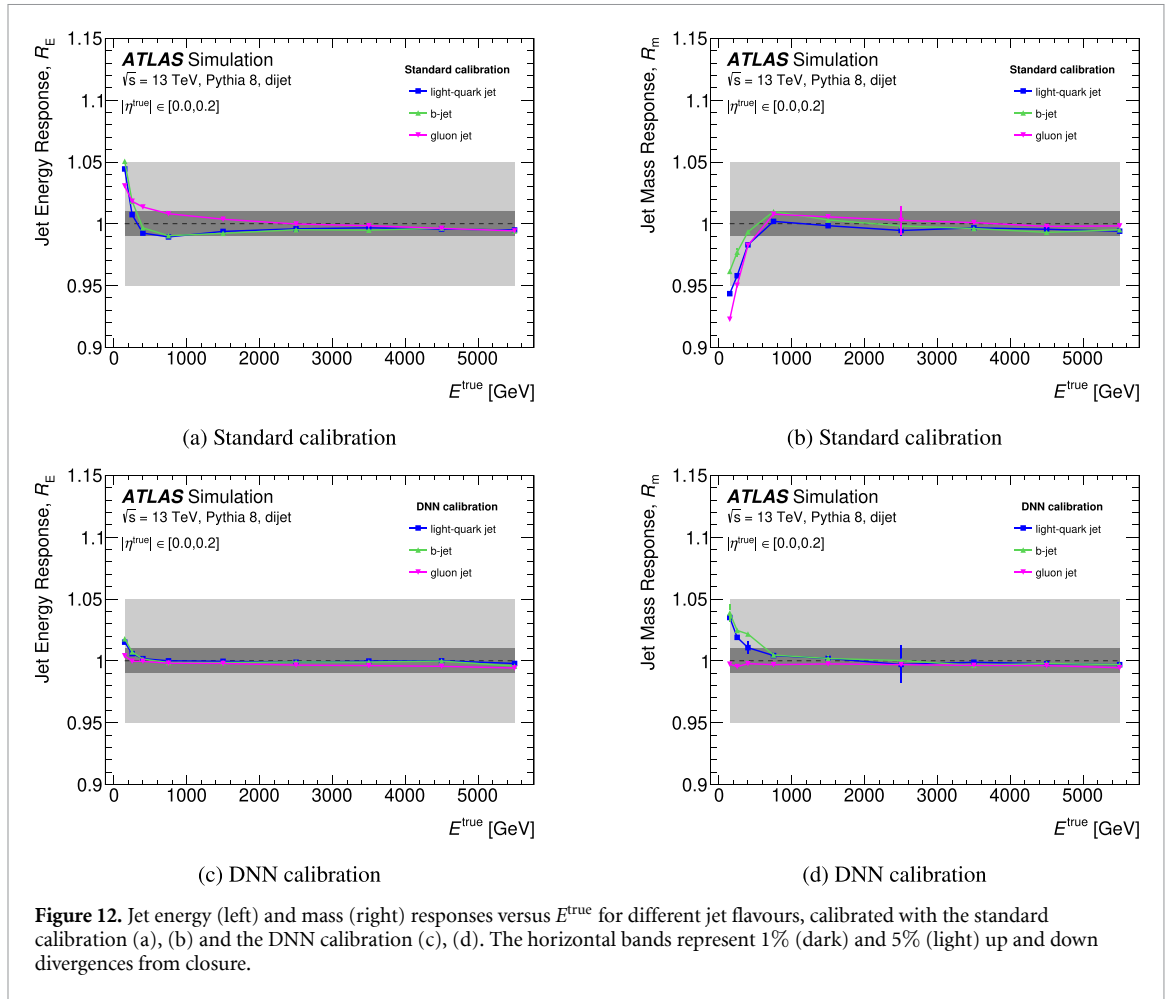


Figure 12. Jet energy (left) and mass (right) responses versus E^{true} for different jet flavours, calibrated with the standard calibration (a), (b) and the DNN calibration (c), (d). The horizontal bands represent 1% (dark) and 5% (light) up and down divergences from closure.

bins. The standard mass calibration shows smaller differences between the two generators but overall, the DNN mass calibration is still better than the standard one for both the PYTHIA and SHERPA generators.

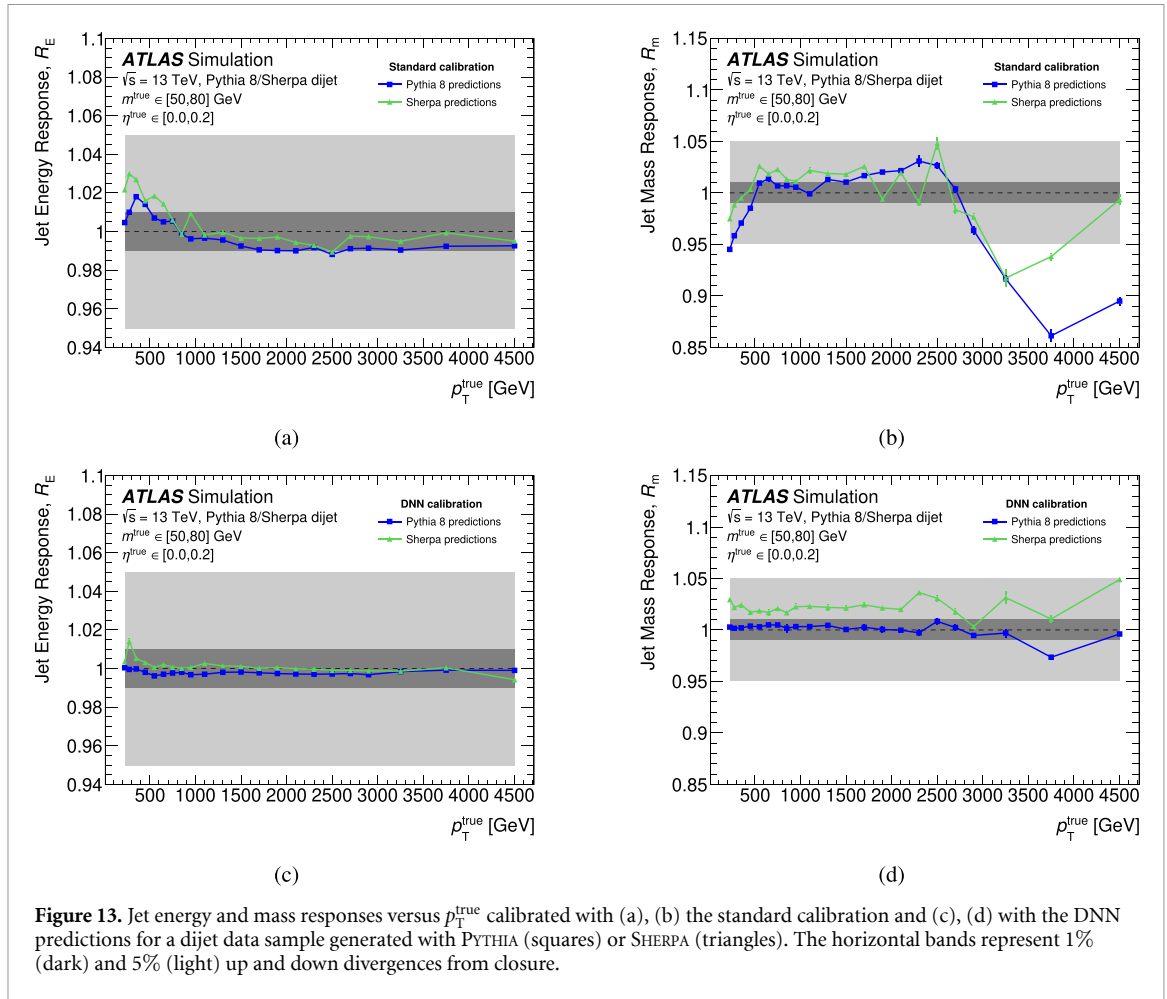
7. Limitations and possible solutions

Despite the satisfying results obtained with the calibration methodology presented above, some limitations and open questions are identified. They are discussed together with possible solutions in this section.

7.1. Training convergence and ending criterion

A weakness in this DNN training procedure is the lack of a clear criterion to mark the final convergence of the network and end the training. It is observed that early interruptions of the training (as soon as the losses start to fluctuate around a minimum) result in worse calibration performance in terms of JES, JMS or resolution in significant parts of the phase space. Instead, training for numerous additional epochs (such as described in section 5.4) during which the training loss remains essentially constant is found to be necessary. A possible explanation is that the goodness of the performance is based on relatively strict expectations (e.g. closure within 1% for the energy response) to be obtained over all the (E, η, m) phase space while only a part of it is statistically dominant in the training sample. As a consequence, the global loss can be mostly determined by this dominant phase space region in which the optimum is quickly reached, while it requires more training to improve the sparsely populated regions. This behaviour also resembles the ‘grokking phenomenon’ observed in some DNN problems where sometimes performance suddenly increases after a very long training period [45].

Although the present study shows that training long enough allows coverage of the full phase space, a robust methodology would require a well-understood criterion to stop the training. Evaluating the calibration performance across all the phase space is not a practical option as it is too costly to perform automatically at each epoch. An interesting approach would be to evaluate the loss in predefined, well-chosen bins (in terms of statistical contents and of physics relevance) of the phase space. Monitoring the



losses in these bins with training and validation samples would possibly be more indicative than monitoring the virtually flat total loss.

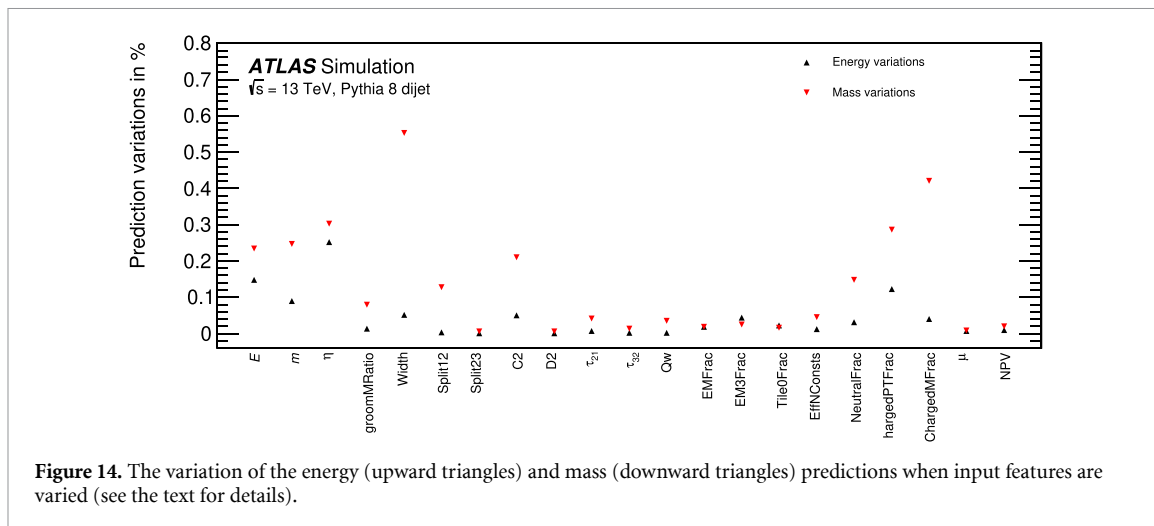
7.2. Calibration of heavy boosted jets

During the validation of the DNN calibration performance for W/Z , Higgs boson and top-quark jets, non-closures of up to a few percent are observed for the energy (see figures 8). While this under-performance is also visible for the standard calibration, the DNN calibration performance is slightly worse in these cases. Contrary to the DNN calibration presented here, the standard calibration is obtained using different types of jets. At high p_T (above ~ 500 GeV) QCD jets are used, while at low p_T the calibration is only derived from W/Z jets as this choice leads to better calibration performance for both W/Z jets and QCD jets.

A similar approach with mixed training samples is possible with the DNN. However, simply adding W/Z samples to the training does not improve—or even degrades—the performance for mass regions away from the W and Z masses. This issue could be mitigated with the availability of special pseudo- W/Z samples having a flat mass distribution. Alternatively, an ad hoc solution mimicking the standard calibration is possible by adding a subnetwork to the already QCD-trained DNN. This subnetwork would branch from the input layer with η annotation, produce output values used as multiplicative correction factors to the main network predictions and enforce these factors to be 1.0 for large p_T jets (typically above 500 GeV) to maintain the good performance of the DNN in this phase space. The subnetwork could then be trained on W/Z samples, while keeping the main network frozen to improve the lower p_T regions.

7.3. Importance of the features

Insights into which input features are the most influential on the DNN predictions are important for two reasons. Firstly, they generally help to understand the jet energy and mass responses. Secondly, they can indicate if some features could be removed from the inputs, potentially leading to a simpler DNN or even to better performance if the removed variables are confusing the network. A simple way to quantify the importance of a feature is to measure the average of the relative variation in the prediction when this feature is systematically varied for each input jet. A ranking of the different features obtained by following this



method is shown in figure 14 where each feature is varied by $\pm 1\%$ of the standard deviation of its overall distribution. Both the energy and mass prediction variations are displayed for each feature. As expected, the variables E , η , and m have a large influence on the predictions according to this measure. Some substructure features¹¹ have a stronger impact on the mass prediction than on the energy prediction. This is also expected since the mass depends on the structure of the particle flow objects in the jet. While by this metric μ and NPV do not seem so important, it was demonstrated in section 6.3 that these features are important as they allow the DNN calibration to remove the response dependence on these variables. Further investigations are therefore necessary to understand more precisely the importance of the features. Those could consist of considering the magnitude of the DNN gradient with respect to its inputs in bins of p_T or mass, or to apply the SHAP methodology¹².

8. Conclusion

A full implementation of a deep neural network based simultaneous calibration of the energy and mass of large- R jets with the ATLAS detector is presented. It solves problems that are specific to the calibration task. Firstly, rather than segmenting the calibration in angular slices, a single network covers multiple detector regions and a dedicated encoding of the jet angular direction is included to help it to adapt to the corresponding strongly varying response. Secondly, the network architecture is designed to efficiently accommodate both the energy and the mass predictions. Finally, loss functions are carefully chosen so that the DNN prediction converges as desired toward the most probable value of the energy or mass response distribution; this also implies non-trivial training procedures involving variants of the loss functions.

The resulting calibration is compared to the standard calibration on QCD jets and on other jet topologies not seen during the DNN training. Over all the phase space and for all processes of interest, the DNN is found to achieve better energy and mass scale closure and similar or better resolution, with a typical 30% improvement in the energy resolution for $p_T > 500$ GeV. The DNN calibration is also shown to be robust against various tests such as pile-up dependency or changes to the sample distribution. Finally, some limitations and possible improvements are discussed. Overall, as this simulation-based method can directly replace the current analogous steps of the ATLAS large- R jet calibration chain, no adaptation of the data-based methodology is required and this DNN procedure can be used for the calibration of large-radius jets used in future ATLAS analyses.

Data availability statement

The data for this manuscript are not available. The values in the plots and tables associated to this article are stored in HEPDATA (<https://www.hepdata.net/>). The data that support the findings of this study are available upon reasonable request from the authors.

¹¹ The Width, groomMRatio, ChargedPTFrac, ChargedMFrac, Split12, and C2.

¹² SHapley Additive exPlanations [46].

Acknowledgments

We thank CERN for the very successful operation of the LHC and its injectors, as well as the support staff at CERN and at our institutions worldwide without whom ATLAS could not be operated efficiently.

The crucial computing support from all WLCG partners is acknowledged gratefully, in particular from CERN the ATLAS Tier-1 facilities at TRIUMF/SFU (Canada), NDGF (Denmark, Norway, Sweden), CC-IN2P3 (France), KIT/GridKA (Germany), INFN-CNAF (Italy), NL-T1 (Netherlands), PIC (Spain), RAL (UK) and BNL (USA), the Tier-2 facilities worldwide and large non-WLCG resource providers. Major contributors of computing resources are listed in [47].

We gratefully acknowledge the support of ANPCyT, Argentina; YerPhI, Armenia; ARC, Australia; BMWFW and FWF, Austria; ANAS, Azerbaijan; CNPq and FAPESP, Brazil; NSERC, NRC and CFI, Canada; CERN; ANID, Chile; CAS, MOST and NSFC, China; Minciencias, Colombia; MEYS CR, Czech Republic; DNRf and DNSRC, Denmark; IN2P3-CNRS and CEA-DRF/IRFU, France; SRNSFG, Georgia; BMBF, HGF and MPG, Germany; GSRI, Greece; RGC and Hong Kong SAR, China; ISF and Benozziyo Center, Israel; INFN, Italy; MEXT and JSPS, Japan; CNRST, Morocco; NWO, Netherlands; RCN, Norway; MEiN, Poland; FCT, Portugal; MNE/IFA, Romania; MESTD, Serbia; MSSR, Slovakia; ARRS and MIZŠ, Slovenia; DSI/NRE, South Africa; MICINN, Spain; SRC and Wallenberg Foundation, Sweden; SERI, SNSF and Cantons of Bern and Geneva, Switzerland; MOST, Taipei; TENMAK, Türkiye; STFC, United Kingdom; DOE and NSF, United States of America.

Individual groups and members have received support from BCKDF, CANARIE, CRC and DRAC, Canada; CERN-CZ, PRIMUS 21/SCI/017 and UNCE SCI/013, Czech Republic; COST, ERC, ERDF, Horizon 2020, ICSC-NextGenerationEU and Marie Skłodowska-Curie Actions, European Union; Investissements d'Avenir Labex, Investissements d'Avenir IDEX and ANR, France; DFG and AvH Foundation, Germany; Herakleitos, Thales and Aristeia programmes co-financed by EU-ESF and the Greek NSRF, Greece; BSF-NSF and MINERVA, Israel; Norwegian Financial Mechanism 2014–2021, Norway; NCN and NAWA, Poland; La Caixa Banking Foundation, CERCA Programme Generalitat de Catalunya and PROMETEO and GenT Programmes Generalitat Valenciana, Spain; Göran Gustafssons Stiftelse, Sweden; The Royal Society and Leverhulme Trust, United Kingdom.

In addition, individual members wish to acknowledge support from CERN: European Organization for Nuclear Research (CERN PJAS); Chile: Agencia Nacional de Investigación y Desarrollo (FONDECYT 1190886, FONDECYT 1210400, FONDECYT 1230987), People's Republic of China: National Natural Science Foundation of China (NSFC—12175119, NSFC 12275265); European Union: European Research Council (ERC—948254, ERC 101089007), Horizon 2020 Framework Programme (MUCCA—CHIST-ERA-19-XAI-00), Italian Center for High Performance Computing, Big Data and Quantum Computing (ICSC, NextGenerationEU), France: Agence Nationale de la Recherche (ANR-20-CE31-0013, ANR-21-CE31-0013, ANR-21-CE31-0022), Investissements d'Avenir Labex (ANR-11-LABX-0012), Germany: Baden-Württemberg Stiftung (BW Stiftung-Postdoc Eliteprogramme), Deutsche Forschungsgemeinschaft (DFG—469666862, DFG—CR 312/5-1), Italy: Istituto Nazionale di Fisica Nucleare (ICSC, NextGenerationEU), Japan: Japan Society for the Promotion of Science (JSPS KAKENHI 22H01227, JSPS KAKENHI 22KK0227, JSPS KAKENHI JP21H05085, JSPS KAKENHI JP22H04944), The Netherlands: Netherlands Organisation for Scientific Research (NWO Veni 2020—VI.Veni.202.179), Norway: Research Council of Norway (RCN-314472); Poland: Polish National Agency for Academic Exchange (PPN/PPO/2020/1/00002/U/00001), Polish National Science Centre (NCN 2021/42/E/ST2/00350, NCN OPUS nr 2022/47/B/ST2/03059, NCN UMO-2019/34/E/ST2/00393, UMO-2020/37/B/ST2/01043, UMO-2021/40/C/ST2/00187, UMO-2022/47/O/ST2/00148), Slovenia: Slovenian Research Agency (ARIS Grant J1-3010), Spain: BBVA Foundation (LEO22-1-603), Generalitat Valenciana (Artemisa, FEDER, IDIFEDER/2018/048), La Caixa Banking Foundation (LCF/BQ/PI20/11760025), Ministry of Science and Innovation (RYC2019-028510-I, RYC2020-030254-I), PROMETEO and GenT Programmes Generalitat Valenciana (CIDEAGENT/2019/023, CIDEAGENT/2019/027); Sweden: Swedish Research Council (VR 2022-03845, VR 2022-04683), Knut and Alice Wallenberg Foundation (KAW 2017.0100, KAW 2018.0157, KAW 2019.0447), Switzerland: Swiss National Science Foundation (SNSF—PCEFP2_194658), United Kingdom: Leverhulme Trust (Leverhulme Trust RPG-2020-004), United States of America: Neubauer Family Foundation.

The ATLAS Collaboration

G Aad¹⁰², E Aakvaag¹⁶, B Abbott¹²⁰, K Abeling⁵⁵, N J Abicht⁴⁹, S H Abidi²⁹,
A Abouhorma^{35e}, H Abramowicz¹⁵¹, H Abreu¹⁵⁰, Y Abulaiti¹¹⁷, B S Acharya^{69a,69b,m},
C Adam Bourdarios⁴, L Adamczyk^{86a}, S V Addepalli²⁶, M J Addison¹⁰¹, J Adelman¹¹⁵,
A Adiguzel^{21c}, T Adye¹³⁴, A A Affolder¹³⁶, Y Afik³⁹, M N Agaras¹³, J Agarwala^{73a,73b},
A Aggarwal¹⁰⁰, C Agheorghiesei^{27c}, A Ahmad³⁶, F Ahmadov^{38,z}, W S Ahmed¹⁰⁴, S Ahuja⁹⁵,
X Ai^{62e}, G Aielli^{76a,76b}, A Aikot¹⁶³, M Ait Tamlihat^{35e}, B Aitbenkikh^{35a}, I Aizenberg¹⁶⁹,
M Akbiyik¹⁰⁰, T P A Åkesson⁹⁸, A V Akimov³⁷, D Akiyama¹⁶⁸, N N Akolkar²⁴, S Aktas^{21a},
K Al Khoury⁴¹, G L Alberghi^{23b}, J Albert¹⁶⁵, P Albicocco⁵³, G L Albouy⁶⁰, S Alderweireldt⁵²,
Z L Alegria¹²¹, M Aleksa³⁶, I N Aleksandrov³⁸, C Alexa^{27b}, T Alexopoulos¹⁰, F Alfonsi^{23b},
M Algren⁵⁶, M Alhroob¹⁴¹, B Ali¹³², H M J Ali⁹¹, S Ali¹⁴⁸, S W Alibocus⁹², M Aliev^{33c},
G Alimonti^{71a}, W Alkakh⁵⁵, C Allaire⁶⁶, B M M Allbrooke¹⁴⁶, J F Allen⁵²,
C A Allendes Flores^{137f}, P P Allport²⁰, A Aloisio^{72a,72b}, F Alonso⁹⁰, C Alpigiani¹³⁸,
M Alvarez Estevez⁹⁹, A Alvarez Fernandez¹⁰⁰, M Alves Cardoso⁵⁶, M G Alviggi^{72a,72b}, M Aly¹⁰¹,
Y Amaral Coutinho^{83b}, A Ambler¹⁰⁴, C Amelung³⁶, M Ameri¹⁰¹, C G Ames¹⁰⁹, D Amidei¹⁰⁶,
S P Amor Dos Santos^{130a}, K R Amos¹⁶³, V Ananiev¹²⁵, C Anastopoulos¹³⁹, T Andeen¹¹,
J K Anders³⁶, S Y Andrean^{47a,47b}, A Andreatza^{71a,71b}, S Angelidakis⁹, A Angerami^{41,ac},
A V Anisenkov³⁷, A Annovi^{74a}, C Antel⁵⁶, M T Anthony¹³⁹, E Antipov¹⁴⁵, M Antonelli⁵³,
F Anulli^{75a}, M Aoki⁸⁴, T Aoki¹⁵³, J A Aparisi Pozo¹⁶³, M A Aparo¹⁴⁶, L Aperio Bella⁴⁸,
C Appelt¹⁸, A Apyan²⁶, S J Arbiol Val⁸⁷, C Arcangeletti⁵³, A T H Arce⁵¹, E Arena⁹²,
J-F Arguin¹⁰⁸, S Argyropoulos⁵⁴, J -H Arling⁴⁸, O Arnaez⁴, H Arnold¹¹⁴, G Artoni^{75a,75b},
H Asada¹¹¹, K Asai¹¹⁸, S Asai¹⁵³, N A Asbah³⁶, K Assamagan²⁹, R Astalos^{28a}, S Atashi¹⁵⁹,
R J Atkin^{33a}, M Atkinson¹⁶², H Atmani^{35f}, P A Atmasiddha¹²⁸, K Augsten¹³², S Auricchio^{72a,72b},
A D Auriol²⁰, V A Austrup¹⁰¹, G Avolio³⁶, K Axiotis⁵⁶, G Azuelos^{108,ag}, D Babal^{28b},
H Bachacou¹³⁵, K Bachas^{152,q}, A Bachiu³⁴, F Backman^{47a,47b}, A Badea³⁹, T M Baer¹⁰⁶,
P Bagnaia^{75a,75b}, M Bahmani¹⁸, D Bahner⁵⁴, K Bai¹²³, A J Bailey¹⁶³, V R Bailey¹⁶²,
J T Baines¹³⁴, L Baines⁹⁴, O K Baker¹⁷², E Bakos¹⁵, D Bakshi Gupta⁸, V Balakrishnan¹²⁰,
R Balasubramanian¹¹⁴, E M Baldin³⁷, P Balek^{86a}, E Ballabene^{23b,23a}, F Balli¹³⁵, L M Baltes^{63a},
W K Balunas³², J Balz¹⁰⁰, E Banas⁸⁷, M Bandieramonte¹²⁹, A Bandyopadhyay²⁴, S Bansal²⁴,
L Barak¹⁵¹, M Barakat⁴⁸, E L Barberio¹⁰⁵, D Barberis^{57b,57a}, M Barbero¹⁰², M Z Barel¹¹⁴,
K N Barends^{33a}, T Barillari¹¹⁰, M-S Barisits³⁶, T Barklow¹⁴³, P Baron¹²²,
D A Baron Moreno¹⁰¹, A Baroncelli^{62a}, G Barone²⁹, A J Barr¹²⁶, J D Barr⁹⁶, F Barreiro⁹⁹,
J Barreiro Guimarães da Costa^{14a}, U Barron¹⁵¹, M G Barros Teixeira^{130a}, S Barsov³⁷, F Bartels^{63a},
R Bartoldus¹⁴³, A E Barton⁹¹, P Bartos^{28a}, A Basan¹⁰⁰, M Baselga⁴⁹, A Bassalat^{66,b},
M J Basso^{156a}, C R Basson¹⁰¹, R L Bates⁵⁹, S Batlamous^{35e}, B Batool¹⁴¹, M Battaglia¹³⁶,
D Battulga¹⁸, M Bauce^{75a,75b}, M Bauer³⁶, P Bauer²⁴, L T Bazzano Hurrell³⁰, J B Beacham⁵¹,
T Beau¹²⁷, J Y Beaucamp⁹⁰, P H Beauchemin¹⁵⁸, P Bechtel²⁴, H P Beck^{19,p}, K Becker¹⁶⁷,
A J Beddall⁸², V A Bednyakov³⁸, C P Bee¹⁴⁵, L J Beemster¹⁵, T A Beermann³⁶, M Begalli^{83d},
M Beger²⁹, A Behera¹⁴⁵, J K Behr⁴⁸, J F Beirer³⁶, F Beisiegel²⁴, M Belfkir^{116b}, G Bella¹⁵¹,
L Bellagamba^{23b}, A Bellerive³⁴, P Bellos²⁰, K Beloborodov³⁷, D Benchevkroun^{35a},
F Bendebba^{35a}, Y Benhammou¹⁵¹, K C Benkendorfer⁶¹, L Beresford⁴⁸, M Beretta⁵³,
E Bergeaas Kuutmann¹⁶¹, N Berger⁴, B Bergmann¹³², J Beringer^{17a}, G Bernardi⁵, C Bernius¹⁴³,
F U Bernlochner²⁴, F Bernon^{36,102}, A Berrocal Guardia¹³, T Berry⁹⁵, P Berta¹³³, A Berthold⁵⁰,
S Bethke¹¹⁰, A Betti^{75a,75b}, A J Bevan⁹⁴, N K Bhalla⁵⁴, M Bhamjee^{33c}, S Bhatta¹⁴⁵,
D S Bhattacharya¹⁶⁶, P Bhattarai¹⁴³, K D Bhide⁵⁴, V S Bhopatkar¹²¹, R M Bianchi¹²⁹,
G Bianco^{23b,23a}, O Biebel¹⁰⁹, R Bielski¹²³, M Biglietti^{77a}, C S Billingsley⁴⁴, M Bindi⁵⁵,
A Bingul^{21b}, C Bini^{75a,75b}, A Biondini⁹², C J Birch-sykes¹⁰¹, G A Bird³², M Birman¹⁶⁹,
M Biros¹³³, S Biryukov¹⁴⁶, T Bisanz⁴⁹, E Bisceglie^{43b,43a}, J P Biswal¹³⁴, D Biswas¹⁴¹,
K Björke¹²⁵, I Bloch⁴⁸, A Blue⁵⁹, U Blumenschein⁹⁴, J Blumenthal¹⁰⁰, V S Bobrovnikov³⁷,
M Boehler⁵⁴, B Boehm¹⁶⁶, D Bogavac³⁶, A G Bogdanchikov³⁷, C Boehm^{47a}, V Boisvert⁹⁵,
P Bokan³⁶, T Bold^{86a}, M Bomben⁵, M Bona⁹⁴, M Boonekamp¹³⁵, C D Booth⁹⁵,
A G Borbély⁵⁹, I S Bordulev³⁷, H M Borecka-Bielska¹⁰⁸, G Borissov⁹¹, D Bortoletto¹²⁶,
D Boscherini^{23b}, M Bosman¹³, J D Bossio Sola³⁶, K Bouaouda^{35a}, N Bouchhar¹⁶³,
J Boudreau¹²⁹, E V Bouhova-Thacker⁹¹, D Boumediene⁴⁰, R Bouquet^{57b,57a}, A Boveia¹¹⁹,
J Boyd³⁶, D Boye²⁹, I R Boyko³⁸, J Bracinik²⁰, N Brahimi⁴, G Brandt¹⁷¹, O Brandt³²,
F Braren⁴⁸, B Brau¹⁰³, J E Brau¹²³, R Brenner¹⁶⁹, L Brenner¹¹⁴, R Brenner¹⁶¹, S Bressler¹⁶⁹,
D Britton⁵⁹, D Britzger¹¹⁰, I Brock²⁴, G Brooijmans⁴¹, E Brost²⁹, L M Brown¹⁶⁵,
L E Bruce⁶¹, T L Bruckler¹²⁶, P A Bruckman de Renstrom⁸⁷, B Brüers⁴⁸, A Bruni^{23b},





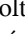


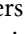
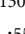
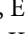

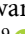


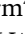
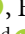

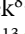
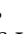




G Bruni^{23b}, M Bruschi^{23b}, N Bruscolo^{75a,75b}, T Buanes¹⁶, Q Buat¹³⁸, D Buchin¹¹⁰,
A G Buckley⁵⁹, O Bulekov³⁷, B A Bullard¹⁴³, S Burdin⁹², C D Burgard⁴⁹, A M Burger³⁶,
B Burghgrave⁸, O Burlayenko⁵⁴, J T P Burr³², C D Burton¹¹, J C Burzynski¹⁴², E L Busch⁴¹,
V Büscher¹⁰⁰, P J Bussey⁵⁹, J M Butler²⁵, C M Buttar⁵⁹, J M Butterworth⁹⁶, W Buttinger¹³⁴,
C J Buxo Vazquez¹⁰⁷, A R Buzykaev³⁷, S Cabrera Urbán¹⁶³, L Cadamuro⁶⁶, D Caforio⁵⁸,
H Cai¹²⁹, Y Cai^{14a,14e}, Y Cai^{14c}, V M M Cairo³⁶, O Cakir^{3a}, N Calace³⁶, P Calafiura^{17a},
G Calderini¹²⁷, P Calfayan⁶⁸, G Callea⁵⁹, L P Caloba^{83b}, D Calvet⁴⁰, S Calvet⁴⁰,
M Calvetti^{74a,74b}, R Camacho Toro¹²⁷, S Camarda³⁶, D Camarero Munoz²⁶, P Camarri^{76a,76b},
M T Camerlingo^{72a,72b}, D Cameron³⁶, C Camincher¹⁶⁵, M Campanelli⁹⁶, A Camplani⁴²,
V Canale^{72a,72b}, A C Canbay^{3a}, J Cantero¹⁶³, Y Cao¹⁶², F Capocasa²⁶, M Capua^{43b,43a},
A Carbone^{71a,71b}, R Cardarelli^{76a}, J C J Cardenas⁸, F Cardillo¹⁶³, G Carducci^{43b,43a}, T Carli³⁶,
G Carlino^{72a}, J I Carlotta¹³, B T Carlson^{129,r}, E M Carlson^{165,156a}, L Carminati^{71a,71b},
A Carnelli¹³⁵, M Carnesale^{75a,75b}, S Caron¹¹³, E Carquin^{137f}, S Carrá^{71a}, G Carratta^{23b,23a},
A M Carroll¹²³, T M Carter⁵², M P Casado^{13,i}, M Caspar⁴⁸, F L Castillo⁴, L Castillo Garcia¹³,
V Castillo Gimenez¹⁶³, N F Castro^{130a,130e}, A Catinaccio³⁶, J R Catmore¹²⁵, T Cavaliere⁴,
V Cavaliere²⁹, N Cavalli^{23b,23a}, Y C Cekmecelioglu⁴⁸, E Celebi^{21a}, F Celli¹²⁶,
M S Centonze^{70a,70b}, V Cepaitis⁵⁶, K Cerny¹²², A S Cerqueira^{83a}, A Cerri¹⁴⁶, L Cerrito^{76a,76b},
F Cerutti^{17a}, B Cervato¹⁴¹, A Cervelli^{23b}, G Cesarini⁵³, S A Cetin⁸², D Chakraborty¹¹⁵,
J Chan^{17a}, W Y Chan¹⁵³, J D Chapman³², E Chapon¹³⁵, B Chargeishvili^{149b}, D G Charlton²⁰,
M Chatterjee¹⁹, C Chauhan¹³³, Y Che^{14c}, S Chekanov⁶, S V Chekulaev^{156a}, G A Chelkov^{38a},
A Chen¹⁰⁶, B Chen¹⁵¹, B Chen¹⁶⁵, H Chen^{14c}, H Chen²⁹, J Chen^{62c}, J Chen¹⁴², M Chen¹²⁶,
S Chen¹⁵³, S J Chen^{14c}, X Chen^{62c,135}, X Chen^{14b,af}, Y Chen^{62a}, C L Cheng¹⁷⁰, H C Cheng^{64a},
S Cheong¹⁴³, A Cheplakov³⁸, E Cheremushkina⁴⁸, E Cherepanova¹¹⁴, R Cherkaoui El Moursli^{35e},
E Cheu⁷, K Cheung⁶⁵, L Chevalier¹³⁵, V Chiarella⁵³, G Chiarelli^{74a}, N Chiedde¹⁰²,
G Chiodini^{70a}, A S Chisholm²⁰, A Chitan^{27b}, M Chitishvili¹⁶³, M V Chizhov³⁸, K Choi¹¹,
Y Chou¹³⁸, E Y S Chow¹¹³, K L Chu¹⁶⁹, M C Chu^{64a}, X Chu^{14a,14e}, J Chudoba¹³¹,
J J Chwastowski⁸⁷, D Cieri¹¹⁰, K M Ciesla^{86a}, V Cindro⁹³, A Ciocio^{17a}, F Ciotto^{72a,72b},
Z H Citron^{169,k}, M Citterio^{71a}, D A Ciubotaru^{27b}, A Clark⁵⁶, P J Clark⁵², C Clarry¹⁵⁵,
J M Clavijo Columbie⁴⁸, S E Clawson⁴⁸, C Clement^{47a,47b}, J Clercx⁴⁸, Y Coadou¹⁰²,
M Cobal^{69a,69c}, A Coccaro^{57b}, R F Coelho Barrue^{130a}, R Coelho Lopes De Sa¹⁰³, S Coelli^{71a},
B Cole⁴¹, J Collot⁶⁰, P Conde Muiño^{130a,130g}, M P Connell^{133c}, S H Connell^{133c}, E I Conroy¹²⁶,
F Conventi^{72a,ah}, H G Cooke²⁰, A M Cooper-Sarkar¹²⁶, A Cordeiro Oudot Choi¹²⁷, L D Corpe⁴⁰,
M Corradi^{75a,75b}, F Corriveau^{104,x}, A Cortes-Gonzalez¹⁸, M J Costa¹⁶³, F Costanza⁴,
D Costanzo¹³⁹, B M Cote¹¹⁹, G Cowan⁹⁵, K Cranmer¹⁷⁰, D Cremonini^{23b,23a},
S Crépe-Renaudin⁶⁰, F Crescioli¹²⁷, M Cristinziani¹⁴¹, M Cristoforetti^{78a,78b}, V Croft¹¹⁴,
J E Crosby¹²¹, G Crosetti^{43b,43a}, A Cueto⁹⁹, T Cuhadar Donszelmann¹⁵⁹, H Cui^{14a,14e}, Z Cui⁷,
W R Cunningham⁵⁹, F Curcio^{43b,43a}, P Czodrowski³⁶, M M Czurylo^{63b},
M J Da Cunha Sargedas De Sousa^{57b,57a}, J V Da Fonseca Pinto^{83b}, C Da Via¹⁰¹, W Dabrowski^{86a},
T Dado⁴⁹, S Dahbi¹⁴⁸, T Dai¹⁰⁶, D Dal Santo¹⁹, C Dallapiccola¹⁰³, M Dam⁴², G D'amen²⁹,
V D'Amico¹⁰⁹, J Damp¹⁰⁰, J R Dandoy³⁴, M Danninger¹⁴², V Dao³⁶, G Darbo^{57b},
S Darmora⁶, S J Das^{29,ai}, S D'Auria^{71a,71b}, A D'Avanzo^{130a}, C David^{133a}, T Davidek¹³³,
B Davis-Purcell³⁴, I Dawson⁹⁴, H A Day-hall¹³², K De⁸, R De Asmundis^{72a}, N De Biase⁴⁸,
S De Castro^{23b,23a}, N De Groot¹¹³, P de Jong¹¹⁴, H De la Torre¹¹⁵, A De Maria^{14c},
A De Salvo^{75a}, U De Sanctis^{76a,76b}, F De Santis^{70a,70b}, A De Santo¹⁴⁶, J B De Vivie De Regie⁶⁰,
D V Dedovich³⁸, J Degens¹¹⁴, A M Deiana⁴⁴, F Del Corso^{23b,23a}, J Del Peso⁹⁹, F Del Rio^{63a},
L Delagrèze¹²⁷, F Deliot¹³⁵, C M Delitzsch⁴⁹, M Della Pietra^{72a,72b}, D Della Volpe⁵⁶,
A Dell'Acqua³⁶, L Dell'Asta^{71a,71b}, M Delmastro⁴, P A Delsart⁶⁰, S Demers¹⁷², M Demichev³⁸,
S P Denisov³⁷, L D'Eramo⁴⁰, D Derendarz⁸⁷, F Derue¹²⁷, P Dervan⁹², K Desch²⁴,
C Deutsch²⁴, F A Di Bello^{57b,57a}, A Di Ciaccio^{76a,76b}, L Di Ciaccio⁴, A Di Domenico^{75a,75b},
C Di Donato^{72a,72b}, A Di Girolamo³⁶, G Di Gregorio³⁶, A Di Luca^{78a,78b}, B Di Micco^{77a,77b},
R Di Nardo^{77a,77b}, M Diamantopoulou³⁴, F A Dias¹¹⁴, T Dias Do Vale¹⁴², M A Diaz^{137a,137b},
F G Diaz Capriles²⁴, M Didenko¹⁶³, E B Diehl¹⁰⁶, S Diez Cornell⁴⁸, C Diez Pardos¹⁴¹,
C Dimitriadi^{161,24}, A Dimitrievska^{17a}, J Dingfelder²⁴, I-M Dinu^{27b}, S J Dittmeier^{63b},
F Dittus³⁶, F Djama¹⁰², T Djobava^{149b}, C Dogliani^{101,98}, A Dohnalova^{28a}, J Dolejsi¹³³,
Z Dolezal¹³³, K M Dona³⁹, M Donadelli^{83c}, B Dong¹⁰⁷, J Donini⁴⁰, A D'Onofrio^{72a,72b},
M D'Onofrio⁹², J Dopke¹³⁴, A Doria^{72a}, N Dos Santos Fernandes^{130a}, P Dougan¹⁰¹,
M T Dova⁹⁰, A T Doyle⁵⁹, M A Draguet¹²⁶, E Dreyer¹⁶⁹, I Drivas-koulouris¹⁰, M Drnevich¹¹⁷,
M Drozdova⁵⁶, D Du^{62a}, T A du Pree¹¹⁴, F Dubinin³⁷, M Dubovsky^{28a}, E Duchovni¹⁶⁹,
G Duckeck¹⁰⁹, O A Ducu^{27b}, D Duda⁵², A Dudarev³⁶, E R Duden²⁶, M D'uffizi¹⁰¹,

L Duflot⁶⁶, M Dührssen³⁶, A E Dumitriu^{27b}, M Dunford^{63a}, S Dungs⁴⁹, K Dunne^{47a,47b}, A Duperrin¹⁰², H Duran Yildiz^{3a}, M Düren⁵⁸, A Durglishvili^{149b}, B L Dwyer¹¹⁵, G I Dyckes^{17a}, M Dyndal^{186a}, B S Dziedzic⁸⁷, Z O Earnshaw¹⁴⁶, G H Eberwein¹²⁶, B Eckerova^{28a}, S Eggebrecht⁵⁵, E Egidio Purcino De Souza¹²⁷, L F Ehrke⁵⁶, G Eigen¹⁶, K Einsweiler^{17a}, T Ekelof¹⁶¹, P A Ekman⁹⁸, S El Farkh^{35b}, Y El Ghazali^{35b}, H El Jarrari³⁶, A El Moussaouy¹⁰⁸, V Ellajosyula¹⁶¹, M Ellert¹⁶¹, F Ellinghaus¹⁷¹, N Ellis³⁶, J Elmsheuser²⁹, M Elsing³⁶, D Emeliyanov¹³⁴, Y Enari¹⁵³, I Ene^{17a}, S Epari¹³, P A Erland⁸⁷, M Errenst¹⁷¹, M Escalier⁶⁶, C Escobar¹⁶³, E Etzion¹⁵¹, G Evans^{130a}, H Evans⁶⁸, L S Evans⁹⁵, A Ezhilov³⁷, S Ezzarqtouni^{35a}, F Fabbri^{23b,23a}, L Fabbri^{23b,23a}, G Facini⁹⁶, V Fadeyev¹³⁶, R M Fakhruddinov³⁷, D Fakoudis¹⁰⁰, S Falciano^{75a}, L F Falda Ulhoa Coelho³⁶, P J Falke²⁴, J Faltova¹³³, C Fan¹⁶², Y Fan^{14a}, Y Fang^{14a,14e}, M Fanti^{71a,71b}, M Faraj^{69a,69b}, Z Farazpay⁹⁷, A Farbin⁸, A Farilla^{77a}, T Farooque¹⁰⁷, S M Farrington⁵², F Fassi^{35c}, D Fassouliotis⁹, M Fauci Giannelli^{76a,76b}, W J Fawcett³², L Fayard⁶⁶, P Federic¹³³, P Federicova¹³¹, O L Fedin^{37a}, M Feickert¹⁷⁰, L Felgioni¹⁰², D E Fellers¹²³, C Feng^{62b}, M Feng^{14b}, Z Feng¹¹⁴, M J Fenton¹⁵⁹, L Ferencz⁴⁸, R A M Ferguson⁹¹, S I Fernandez Luengo^{137f}, P Fernandez Martinez¹³, M J V Fernoux¹⁰², J Ferrando⁹¹, A Ferrari¹⁶¹, P Ferrari^{114,113}, R Ferrari^{73a}, D Ferrere⁵⁶, C Ferretti¹⁰⁶, F Fiedler¹⁰⁰, P Fiedler¹³², A Filipčić⁹³, E K Filmer¹, F Filthaut¹¹³, M C N Fiolhais^{130a,130c,c}, L Fiorini¹⁶³, W C Fisher¹⁰⁷, T Fitschen¹⁰¹, P M Fitzhugh¹³⁵, I Fleck¹⁴¹, P Fleischmann¹⁰⁶, T Flick¹⁷¹, M Flores^{33d,ad}, L R Flores Castillo^{64a}, L Flores Sanz De Acedo³⁶, F M Follega^{78a,78b}, N Fomin¹⁶, J H Foo¹⁵⁵, A Formica¹³⁵, A C Forti¹⁰¹, E Fortin³⁶, A W Fortman^{17a}, M G Foti^{17a}, L Fountas^{9j}, D Fournier⁶⁶, H Fox⁹¹, P Francavilla^{74a,74b}, S Francescato⁶¹, S Franchellucci⁵⁶, M Franchini^{23b,23a}, S Franchino^{63a}, D Francis³⁶, L Franco¹¹³, V Franco Lima³⁶, L Franconi⁴⁸, M Franklin⁶¹, G Frattari²⁶, W S Freund^{83b}, Y Y Frid¹⁵¹, J Friend⁵⁹, N Fritzsche⁵⁰, A Froch⁵⁴, D Froidevaux³⁶, J A Frost¹²⁶, Y Fu^{62a}, S Fuenzalida Garrido^{137f}, M Fujimoto¹⁰², K Y Fung^{64a}, E Furtado De Simas Filho^{83b}, M Furukawa¹⁵³, J Fuster¹⁶³, A Gabrielli^{23b,23a}, A Gabrielli¹⁵⁵, P Gadow³⁶, G Gagliardi^{57b,57a}, L G Gagnon^{17a}, S Galantzan¹⁵¹, E J Gallas¹²⁶, B J Gallop¹³⁴, K K Gan¹¹⁹, S Ganguly¹⁵³, Y Gao⁵², F M Garay Walls^{137a,137b}, B Garcia²⁹, C García¹⁶³, A Garcia Alonso¹¹⁴, A G Garcia Caffaro¹⁷², J E García Navarro¹⁶³, M Garcia-Sciveres^{17a}, G L Gardner¹²⁸, R W Gardner³⁹, N Garelli¹⁵⁸, D Garg⁸⁰, R B Garg^{143,n}, J M Gargan⁵², C A Garner¹⁵⁵, C M Garvey^{33a}, P Gaspar^{83b}, V K Gassmann¹⁵⁸, G Gaudio^{73a}, V Gautam¹³, P Gauzzi^{75a,75b}, I L Gavrilenko³⁷, A Gavrilyuk³⁷, C Gay¹⁶⁴, G Gaycken⁴⁸, E N Gazis¹⁰, A A Geanta^{27b}, C M Gee¹³⁶, A Gekow¹¹⁹, C Gemme^{57b}, M H Genest⁶⁰, A D Gentry¹¹², S George⁹⁵, W F George²⁰, T Geralis⁴⁶, P Gessinger-Befurt³⁶, M E Geyik¹⁷¹, M Ghani¹⁶⁷, M Ghneimat¹⁴¹, K Ghorbanian⁹⁴, A Ghosal¹⁴¹, A Ghosh¹⁵⁹, A Ghosh⁷, B Giacobbe^{23b}, S Giagu^{75a,75b}, T Giani¹¹⁴, P Giannetti^{74a}, A Giannini^{62a}, S M Gibson⁹⁵, M Gignac¹³⁶, D T Gil^{86b}, A K Gilbert^{86a}, B J Gilbert⁴¹, D Gillberg³⁴, G Gilles¹¹⁴, L Ginabat¹²⁷, D M Gingrich^{2,ag}, M P Giordani^{69a,69c}, P F Giraud¹³⁵, G Giugliarelli^{69a,69c}, D Giugni^{71a}, F Giuli³⁶, I Gkialas^{9j}, L K Gladilin³⁷, C Glasman⁹⁹, G R Gledhill¹²³, G Glemža⁴⁸, M Glisic¹²³, I Gnesi^{43b,f}, Y Go²⁹, M Goblirsch-Kolb³⁶, B Gocke⁴⁹, D Godin¹⁰⁸, B Gokturk^{21a}, S Goldfarb¹⁰⁵, T Golling⁵⁶, M G D Gololo^{33g}, D Golubkov³⁷, J P Gombas¹⁰⁷, A Gomes^{130a,130b}, G Gomes Da Silva¹⁴¹, A J Gomez Delegido¹⁶³, R Gonçalves^{130a,130c}, L Gonella²⁰, A Gongadze^{149c}, F Gonnella²⁰, J L Gonski¹⁴³, R Y González Andana⁵², S González de la Hoz¹⁶³, R Gonzalez Lopez⁹², C Gonzalez Renteria^{17a}, M V Gonzalez Rodrigues⁴⁸, R Gonzalez Suarez¹⁶¹, S Gonzalez-Sevilla⁵⁶, G R Gonzalvo Rodriguez¹⁶³, L Goossens³⁶, B Gorini³⁶, E Gorini^{70a,70b}, A Gorišek⁹³, T C Gosart¹²⁸, A T Goshaw⁵¹, M I Gostkin³⁸, S Goswami¹²¹, C A Gottardo³⁶, S A Gotz¹⁰⁹, M Gouighri^{35b}, V Goumarre⁴⁸, A G Goussiou¹³⁸, N Govender^{33c}, I Grabowska-Bold^{86a}, K Graham³⁴, E Gramstad¹²⁵, S Grancagnolo^{70a,70b}, C M Grant^{1,135}, P M Gravila^{27f}, F G Gravili^{70a,70b}, H M Gray^{17a}, M Greco^{70a,70b}, C Grefe²⁴, I M Gregor⁴⁸, P Grenier¹⁴³, S G Grewe¹¹⁰, A A Grillo¹³⁶, K Grimm³¹, S Grinstein^{13,t}, J -F Grivaz⁶⁶, E Gross¹⁶⁹, J Grosse-Knetter⁵⁵, J C Grundy¹²⁶, L Guan¹⁰⁶, C Gubbels¹⁶⁴, J G R Guerrero Rojas¹⁶³, G Guerrieri^{69a,69c}, F Guescini¹¹⁰, R Gugel¹⁰⁰, J A M Guhit¹⁰⁶, A Guida¹⁸, E Guilloton¹⁶⁷, S Guindon³⁶, F Guo^{14a,14e}, J Guo^{62c}, L Guo⁴⁸, Y Guo¹⁰⁶, R Gupta⁴⁸, R Gupta¹²⁹, S Gurbuz²⁴, S S Gurdasani⁵⁴, G Gustavino³⁶, M Guth⁵⁶, P Gutierrez¹²⁰, L F Gutierrez Zagazeta¹²⁸, M Gutsche⁵⁰, C Gutschow⁹⁶, C Gwenlan¹²⁶, C B Gwilliam⁹², E S Haaland¹²⁵, A Haas¹¹⁷, M Habedank⁴⁸, C Haber^{17a}, H K Hadavand⁸, A Hadeef⁵⁰, S Hadzic¹¹⁰, A I Hagan⁹¹, J J Hahn¹⁴¹, E H Haines⁹⁶, M Haleem¹⁶⁶, J Haley¹²¹, J J Hall¹³⁹, G D Hallewell¹⁰², L Halser¹⁹, K Hamano¹⁶⁵, M Hamer²⁴, G N Hamity⁵², E J Hampshire⁹⁵, J Han^{62b}, K Han^{62a}, L Han^{14c}, L Han^{62a}, S Han^{17a}, Y F Han¹⁵⁵, K Hanagaki⁸⁴, M Hance¹³⁶

D A Hangal⁴¹, H Hanif¹⁴², M D Hank¹²⁸, J B Hansen⁴², P H Hansen⁴², K Hara¹⁵⁷,
D Harada⁵⁶, T Harenberg¹⁷¹, S Harkusha³⁷, M L Harris¹⁰³, Y T Harris¹²⁶, J Harrison¹³,
N M Harrison¹¹⁹, P F Harrison¹⁶⁷, N M Hartman¹¹⁰, N M Hartmann¹⁰⁹, Y Hasegawa¹⁴⁰,
R Hauser¹⁰⁷, C M Hawkes²⁰, R J Hawkings³⁶, Y Hayashi¹⁵³, S Hayashida¹¹¹, D Hayden¹⁰⁷,
C Hayes¹⁰⁶, R L Hayes¹¹⁴, C P Hays¹²⁶, J M Hays⁹⁴, H S Hayward⁹², F He^{62a}, M He^{14a,14e},
Y He¹⁵⁴, Y He⁴⁸, Y He⁹⁶, N B Heatley⁹⁴, V Hedberg⁹⁸, A L Heggelund¹²⁵, N D Hehir^{94,†},
C Heidegger⁵⁴, K K Heidegger⁵⁴, W D Heidorn⁸¹, J Heilman³⁴, S Heim⁴⁸, T Heim^{17a},
J G Heinlein¹²⁸, J J Heinrich¹²³, L Heinrich^{110,ac}, J Hejbal¹³¹, A Held¹⁷⁰, S Hellesund¹⁶,
C M Helling¹⁶⁴, S Hellman^{47a,47b}, R C W Henderson⁹¹, L Henkelmann³², A M Henriques Correia³⁶,
H Herde⁹⁸, Y Hernández Jiménez¹⁴⁵, L M Herrmann²⁴, T Herrmann⁵⁰, G Herten⁵⁴,
R Hertenberger¹⁰⁹, L Hervas³⁶, M E Hesping¹⁰⁰, N P Hessey^{156a}, E Hill¹⁵⁵, S J Hillier²⁰,
J R Hinds¹⁰⁷, F Hinterkeuser²⁴, M Hirose¹²⁴, S Hirose¹⁵⁷, D Hirschbuehl¹⁷¹, T G Hitchings¹⁰¹,
B Hiti⁹³, J Hobbs¹⁴⁵, R Hobincu^{27c}, N Hod¹⁶⁹, M C Hodgkinson¹³⁹, B H Hodgkinson¹²⁶,
A Hoecker³⁶, D D Hofer¹⁰⁶, J Hofer⁴⁸, T Holm²⁴, M Holzbock¹¹⁰, L B A H Hommels³²,
B P Honan¹⁰¹, J Hong^{62c}, T M Hong¹²⁹, B H Hooberman¹⁶², W H Hopkins⁶, Y Horii¹¹¹,
S Hou¹⁴⁸, A S Howard⁹³, J Howarth⁵⁹, J Hoya⁶, M Hrabovsky¹²², A Hrynevich⁴⁸,
T Hryn'ova⁴, P J Hsu⁶⁵, S -C Hsu¹³⁸, Q Hu^{62a}, S Huang^{64b}, X Huang^{14c}, X Huang^{14a,14e},
Y Huang¹³⁹, Y Huang^{14a}, Z Huang¹⁰¹, Z Hubacek¹³², M Huebner²⁴, F Huegging²⁴,
T B Huffman¹²⁶, C A Hugli⁴⁸, M Huhtinen³⁶, S K Huiberts¹⁶, R Hulsken¹⁰⁴, N Huseynov¹²,
J Huston¹⁰⁷, J Huth⁶¹, R Hyneman¹⁴³, G Iacobucci⁵⁶, G Iakovidis²⁹, I Ibragimov¹⁴¹,
L Iconomidou-Fayard⁶⁶, J P Iddon³⁶, P Inengo^{72a,72b}, R Iguchi¹⁵³, T Iizawa¹²⁶, Y Ikegami⁸⁴,
N Ilic¹⁵⁵, H Imam^{35a}, M Ince Lezki⁵⁶, T Ingebretsen Carlson^{47a,47b}, G Introzzi^{73a,73b},
M Iodice^{77a}, V Ippolito^{75a,75b}, R K Irwin⁹², M Ishino¹⁵³, W Islam¹⁷⁰, C Issever^{18,48},
S Istin^{21a,ak}, H Ito¹⁶⁸, R Iuppa^{78a,78b}, A Ivina¹⁶⁹, J M Izen⁴⁵, V Izzo^{72a}, P Jacka^{131,132},
P Jackson¹, B P Jaeger¹⁴², C S Jagfeld¹⁰⁹, G Jain^{156a}, P Jain⁵⁴, K Jakobs⁵⁴, T Jakoubek¹⁶⁹,
J Jamieson⁵⁹, K W Janas^{86a}, M Javurkova¹⁰³, L Jeanty¹²³, J Jejelava^{149a,aa}, P Jenni^{54,g},
C E Jessiman³⁴, C Jia^{62b}, J Jia¹⁴⁵, X Jia⁶¹, X Jia^{14a,14e}, Z Jia^{14c}, S Jiggins⁴⁸, J Jimenez Pena¹³,
S Jin^{14c}, A Jinaru^{27b}, O Jinnouchi¹⁵⁴, P Johansson¹³⁹, K A Johns⁷, J W Johnson¹³⁶,
D M Jones³², E Jones⁴⁸, P Jones³², R W L Jones⁹¹, T J Jones⁹², H L Joos^{55,36}, R Joshi¹¹⁹,
J Jovicevic¹⁵, X Ju^{17a}, J J Junggeburth¹⁰³, T Junkermann^{63a}, A Juste Rozas^{13,t}, M K Juzek⁸⁷,
S Kabana^{137e}, A Kaczmarska⁸⁷, M Kado¹¹⁰, H Kagan¹¹⁹, M Kagan¹⁴³, A Kahn⁴¹, A Kahn¹²⁸,
C Kahra¹⁰⁰, T Kaji¹⁵³, E Kajomovitz¹⁵⁰, N Kakati¹⁶⁹, I Kalaitzidou⁵⁴, C W Kalderon²⁹,
N J Kang¹³⁶, D Kar^{33g}, K Karava¹²⁶, M J Kareem^{156b}, E Karentzos⁵⁴, I Karkanias¹⁵²,
O Karkout¹¹⁴, S N Karpov³⁸, Z M Karpova³⁸, V Kartvelishvili⁹¹, A N Karyukhin³⁷, E Kasimi¹⁵²,
J Katzy⁴⁸, S Kaur³⁴, K Kawade¹⁴⁰, M P Kawale¹²⁰, C Kawamoto⁸⁸, T Kawamoto^{62a},
E F Kay³⁶, F I Kaya¹⁵⁸, S Kazakos¹⁰⁷, V F Kazanin³⁷, Y Ke¹⁴⁵, J M Keaveney^{33a}, R Keeler¹⁶⁵,
G V Kehris⁶¹, J S Keller³⁴, A S Kelly⁹⁶, J J Kempster¹⁴⁶, P D Kennedy¹⁰⁰, O Kepka¹³¹,
B P Kerridge¹³⁴, S Kersten¹⁷¹, B P Kerševan⁹³, S Keshri⁶⁶, L Keszeghova^{28a},
S Ketabchi Haghighat¹⁵⁵, R A Khan¹²⁹, A Khanov¹²¹, A G Kharlamov³⁷, T Kharlamova³⁷,
E E Khoda¹³⁸, M Kholodenko³⁷, T J Khoo¹⁸, G Khoraiuli¹⁶⁶, J Khubua^{149b}, Y A R Khwaira⁶⁶,
B Kibirige^{33g}, A Kilgallon¹²³, D W Kim^{47a,47b}, Y K Kim³⁹, N Kimura⁹⁶, M K Kingston⁵⁵,
A Kirchner⁵⁵, C Kirfel²⁴, F Kirfel²⁴, J Kirk¹³⁴, A E Kiryunin¹¹⁰, C Kitsaki¹⁰, O Kivernyk²⁴,
M Klassen^{63a}, C Klein³⁴, L Klein¹⁶⁶, M H Klein⁴⁴, S B Klein⁵⁶, U Klein⁹², P Klimek³⁶,
A Klimentov²⁹, T Klioutchnikova³⁶, P Kluit¹¹⁴, S Kluth¹¹⁰, E Kneringer⁷⁹, T M Knight¹⁵⁵,
A Knue⁴⁹, R Kobayashi⁸⁸, D Kobylanski¹⁶⁹, S F Koch¹²⁶, M Kocian¹⁴³, P Kodyš¹³³,
D M Koeck¹²³, P T Koenig²⁴, T Koffas³⁴, O Kolay⁵⁰, I Koletsou⁴, T Komarek¹²², K Köneke⁵⁴,
A X Y Kong¹, T Kono¹¹⁸, N Konstantinidis⁹⁶, P Kontaxakis⁵⁶, B Konya⁹⁸, R Kopeliansky⁶⁸,
S Koperny^{86a}, K Korcyl⁸⁷, K Kordas^{152,e}, A Korn⁹⁶, S Korn⁵⁵, I Korolkov¹³, N Korotkova³⁷,
B Kortman¹¹⁴, O Kortner¹¹⁰, S Kortner¹¹⁰, W H Kostecka¹¹⁵, V V Kostyukhin¹⁴¹,
A Kotskechagia¹³⁵, A Kotwal⁵¹, A Koulouris³⁶, A Kourkoumeli-Charalampidi^{73a,73b},
C Kourkoumelis⁹, E Kourlitis^{110,ac}, O Kovanda¹²³, R Kowalewski¹⁶⁵, W Kozanecki¹³⁵,
A S Kozhin³⁷, V A Kramarenko³⁷, G Kramberger⁹³, P Kramer¹⁰⁰, M W Krasny¹²⁷,
A Krasznahorkay³⁶, J W Kraus¹⁷¹, J A Kremer⁴⁸, T Kresse⁵⁰, J Kretschmar⁹², K Kreul¹⁸,
P Krieger¹⁵⁵, S Krishnamurthy¹⁰³, M Krivos¹³³, K Krizka²⁰, K Kroeninger⁴⁹, H Kroha¹¹⁰,
J Kroll¹³¹, J Kroll¹²⁸, K S Krowpman¹⁰⁷, U Kruchonak³⁸, H Krüger²⁴, N Krumnack⁸¹,
M C Kruse⁵¹, O Kuchinskaia³⁷, S Kuday^{3a}, S Kuehn³⁶, R Kuesters⁵⁴, T Kuhl⁴⁸, V Kukhtin³⁸,
Y Kulchitsky^{37,a}, S Kuleshov^{137d,137b}, M Kumar^{33g}, N Kumari⁴⁸, P Kumari^{156b}, A Kupco¹³¹,
T Kupfer⁴⁹, A Kupich³⁷, O Kuprash⁵⁴, H Kurashige⁸⁵, L L Kurchaninov^{156a}, O Kurdyshev⁶⁶,
Y A Kurochkin³⁷, A Kurova³⁷, M Kuze¹⁵⁴, A K Kvam¹⁰³, J Kvita¹²², T Kwan¹⁰⁴,

M Morinaga¹⁵³, F Morodei^{75a,75b}, L Morvaj³⁶, P Moschovakos³⁶, B Moser³⁶, M Mosidze^{149b}, T Moskalets⁵⁴, P Moskvitina¹¹³, J Moss^{31,i}, A Moussa^{35d}, E J W Moyses¹⁰³, O Mtintsilana^{33g}, S Muanza¹⁰², J Mueller¹²⁹, D Muenstermann⁹¹, R Müller¹⁹, G A Mullier¹⁶¹, A J Mullin³², J J Mullin¹²⁸, D P Mungo¹⁵⁵, D Munoz Perez¹⁶³, F J Munoz Sanchez¹⁰¹, M Murin¹⁰¹, W J Murray^{167,134}, M Muškinja⁹³, C Mwewa²⁹, A G Myagkov^{37,a}, A J Myers⁸, G Myers¹⁰⁶, M Myska¹³², B P Nachman^{17a}, O Nackenhorst⁴⁹, K Nagai¹²⁶, K Nagano⁸⁴, J L Nagle^{29,ai}, E Nagy¹⁰², A M Nairz³⁶, Y Nakahama⁸⁴, K Nakamura⁸⁴, K Nakkalil⁵, H Nanjo¹²⁴, R Narayan⁴⁴, E A Narayanan¹¹², I Naryshkin³⁷, M Naseri³⁴, S Nasri^{116b}, C Nass²⁴, G Navarro^{22a}, J Navarro-Gonzalez¹⁶³, R Nayak¹⁵¹, A Nayaz¹⁸, P Y Nechaeva³⁷, F Nechansky⁴⁸, L Nedic¹²⁶, T J Neep²⁰, A Negri^{73a,73b}, M Negrini^{23b}, C Nellist¹¹⁴, C Nelson¹⁰⁴, K Nelson¹⁰⁶, S Nemecek¹³¹, M Nessi^{36,h}, M S Neubauer¹⁶², F Neuhaus¹⁰⁰, J Neundorfer⁴⁸, R Newhouse¹⁶⁴, P R Newman²⁰, C W Ng¹²⁹, Y W Y Ng⁴⁸, B Ngair^{116a}, H D N Nguyen¹⁰⁸, R B Nickerson¹²⁶, R Nicolaidou¹³⁵, J Nielsen¹³⁶, M Niemeyer⁵⁵, J Niermann⁵⁵, N Nikiforou³⁶, V Nikolaenko^{37,a}, I Nikolic-Audit¹²⁷, K Nikolopoulos²⁰, P Nilsson²⁹, I Ninca⁴⁸, H R Nindhito⁵⁶, G Ninio¹⁵¹, A Nisati^{75a}, N Nishu², R Nisius¹¹⁰, J-E Nitschke⁵⁰, E K Nkadimeng^{33g}, T Nobe¹⁵³, D L Noel³², T Nommensen¹⁴⁷, M B Norfolk¹³⁹, R R B Norisam⁹⁶, B J Norman³⁴, M Noury^{35a}, J Novak⁹³, T Novak⁴⁸, L Novotny¹³², R Novotny¹¹², L Nozka¹²², K Ntekas¹⁵⁹, N M J Nunes De Moura Junior^{83b}, J Ocariz¹²⁷, A Ochi⁸⁵, I Ochoa^{130a}, S Oerdek^{48,u}, J T Offermann³⁹, A Ogrodnik¹³³, A Oh¹⁰¹, C C Ohm¹⁴⁴, H Oide⁸⁴, R Oishi¹⁵³, M L Ojeda⁴⁸, Y Okumura¹⁵³, L F Oleiro Seabra^{130a}, S A Olivares Pino^{137d}, D Oliveira Damazio²⁹, D Oliveira Goncalves^{83a}, J L Oliver¹⁵⁹, Ö O Öncel⁵⁴, A P O'Neill¹⁹, A Onofre^{130a,130c}, P U E Onyisi¹¹, M J Oreglia³⁹, G E Orellana⁹⁰, D Orestano^{77a,77b}, N Orlando¹³, R S Orr¹⁵⁵, V O'Shea⁵⁹, L M Osojinak¹²⁸, R Ospanov^{62a}, G Otero y Garzon³⁰, H Otono⁸⁹, P S Ott^{63a}, G J Ottino^{17a}, M Ouchrif^{35d}, F Ould-Saada¹²⁵, M Owen⁵⁹, R E Owen¹³⁴, K Y Oyulmaz^{21a}, V E Ozcan^{21a}, F Ozturk⁸⁷, N Ozturk⁸, S Ozturk⁸², H A Pacey¹²⁶, A Pacheco Pages¹³, C Padilla Aranda¹³, G Padovano^{75a,75b}, S Pagan Griso^{17a}, G Palacino⁶⁸, A Palazzo^{70a,70b}, J Pampel²⁴, J Pan¹⁷², T Pan^{64a}, D K Panchal¹¹, C E Pandini¹¹⁴, J G Panduro Vazquez⁹⁵, H D Pandya¹, H Pang^{14b}, P Pani⁴⁸, G Panizzo^{69a,69c}, L Panwar¹²⁷, L Paolozzi⁵⁶, S Parajuli¹⁶², A Paramonov⁶, C Paraskevopoulos⁵³, D Paredes Hernandez^{64b}, A Pareti^{73a,73b}, K R Park⁴¹, T H Park¹⁵⁵, M A Parker³², F Parodi^{57b,57a}, E W Parrish¹¹⁵, V A Parrish⁵², J A Parsons⁴¹, U Parzefall⁵⁴, B Pascual Dias¹⁰⁸, L Pascual Dominguez¹⁵¹, E Pasqualucci^{75a}, S Passaggio^{57b}, F Pastore⁹⁵, P Patel⁸⁷, U M Patel⁵¹, J R Pater¹⁰¹, T Pauly³⁶, C I Pazos¹⁵⁸, J Pearkes¹⁴³, M Pedersen¹²⁵, R Pedro^{130a}, S V Peleganchuk³⁷, O Penc³⁶, E A Pender⁵², G D Penn¹⁷², K E Penski¹⁰⁹, M Penzin³⁷, B S Peralva^{83d}, A P Pereira Peixoto⁶⁰, L Pereira Sanchez¹⁴³, D V Perpelitsa^{29,ai}, E Perez Codina^{156a}, M Perganti¹⁰, H Pernegger³⁶, O Perrin⁴⁰, K Peters⁴⁸, R F Y Peters¹⁰¹, B A Petersen³⁶, T C Petersen⁴², E Petit¹⁰², V Petousis¹³², C Petridou^{152,c}, T Petru¹³³, A Petrukhin¹⁴¹, M Pettec^{17a}, N E Pettersson³⁶, A Petukhov³⁷, K Petukhova¹³³, R Pezoa^{137f}, L Pezzotti³⁶, G Pezzullo¹⁷², T M Pham¹⁷⁰, T Pham¹⁰⁵, P W Phillips¹³⁴, G Piacquadio¹⁴⁵, E Pianori^{17a}, F Piazza¹²³, R Piegai³⁰, D Pietreanu^{27b}, A D Pilkington¹⁰¹, M Pinamonti^{69a,69c}, J L Pinfold², B C Pinheiro Pereira^{130a}, A E Pinto Pinoargote^{100,135}, L Pintucci^{69a,69c}, K M Piper¹⁴⁶, A Pirttikoski⁵⁶, D A Pizzi³⁴, L Pizzimento^{64b}, A Pizzini¹¹⁴, M -A Pleier²⁹, V Plesanovs⁵⁴, V Pleskot¹³³, E Plotnikova³⁸, G Poddar⁹⁴, R Poettgen⁹⁸, L Poggioni¹²⁷, I Pokharel⁵⁵, S Polacek¹³³, G Polesello^{73a}, A Poley^{142,156a}, A Polini^{23b}, C S Pollard¹⁶⁷, Z B Pollock¹¹⁹, E Pompa Pacchi^{75a,75b}, D Ponomarenko¹¹³, L Pontecorvo³⁶, S Popa^{27a}, G A Popeneci^{27d}, A Poreba³⁶, D M Portillo Quintero^{156a}, S Pospisil¹³², M A Postill¹³⁹, P Postolache^{27c}, K Potamianos¹⁶⁷, P A Potepa^{86a}, I N Potrap³⁸, C J Potter³², H Potti¹, T Poulsen⁴⁸, J Poveda¹⁶³, M E Pozo Astigarraga³⁶, A Prades Ibanez¹⁶³, J Pretel⁵⁴, D Price¹⁰¹, M Primavera^{70a}, M A Principe Martin⁹⁹, R Privara¹²², T Procter⁵⁹, M L Proffitt¹³⁸, N Proklova¹²⁸, K Prokofiev^{64c}, G Proto¹¹⁰, J Proudfoot⁶, M Przybycien^{86a}, W W Przygoda^{86b}, A Psallidas⁴⁶, J E Puddefoot¹³⁹, D Pudzha³⁷, D Pyatiizbyantseva³⁷, J Qian¹⁰⁶, D Qichen¹⁰¹, Y Qin¹⁰¹, T Qiu⁵², A Quadt⁵⁵, M Queitsch-Maitland¹⁰¹, G Quetant⁵⁶, R P Quinn¹⁶⁴, G Rabanal Bolanos⁶¹, D Rafanoharana⁵⁴, F Ragusa^{71a,71b}, J L Rainbolt³⁹, J A Raine⁵⁶, S Rajagopalan²⁹, E Ramakoti³⁷, I A Ramirez-Berend³⁴, K Ran^{48,14c}, N P Rapheeha^{33g}, H Rasheed^{27b}, V Raskina¹²⁷, D F Rassloff^{63a}, A Rastogi^{17a}, S Rave¹⁰⁰, B Ravina⁵⁵, I Ravinovich¹⁶⁹, M Raymond³⁶, A L Read¹²⁵, N P Radioff¹³⁹, D M Rebuffi^{73a,73b}, G Redlinger²⁹, A S Reed¹¹⁰, K Reeves²⁶, J A Reidelsturz¹⁷¹, D Reikher¹⁵¹, A Rej⁴⁹, C Rembser³⁶, M Renda^{27b}, M B Rendel¹¹⁰, F Renner⁴⁸, A G Rennie¹⁵⁹, A L Rescia⁴⁸, S Resconi^{71a}, M Ressegotti^{57b,57a}, S Rettie³⁶, J G Reyes Rivera¹⁰⁷, E Reynolds^{17a}, O L Rezanova³⁷, P Reznicek¹³³, H Riani^{35d}, N Ribaric⁹¹, E Ricci^{78a,78b}, R Richter¹¹⁰,

J Strandberg¹⁴⁴, S Strandberg^{47a,47b}, M Stratmann¹⁷¹, M Strauss¹²⁰, T Strebler¹⁰²,
P Strizenec^{28b}, R Ströhmer¹⁶⁶, D M Strom¹²³, R Stroynowski⁴⁴, A Strubig^{47a,47b}, S A Stucci²⁹,
B Stugu¹⁶, J Stupak¹²⁰, N A Styles⁴⁸, D Su¹⁴³, S Su^{62a}, W Su^{62d}, X Su^{62a}, D Suchy^{28a},
K Sugizaki¹⁵³, V V Sulin³⁷, M J Sullivan⁹², D M S Sultan¹²⁶, L Sultanaliyeva³⁷, S Sultansoy^{3b},
T Sumida⁸⁸, S Sun¹⁰⁶, S Sun¹⁷⁰, O Sunneborn Gudnadottir¹⁶¹, N Sur¹⁰², M R Sutton¹⁴⁶,
H Suzuki¹⁵⁷, M Svatos¹³¹, M Swiatlowski^{156a}, T Swirski¹⁶⁶, I Sykora^{28a}, M Sykora¹³³,
T Sykora¹³³, D Ta¹⁰⁰, K Tackmann^{48,u}, A Taffard¹⁵⁹, R Tafirout^{156a}, J S Tafoya Vargas⁶⁶,
Y Takuba⁸⁴, M Talby¹⁰², A A Talyshv³⁷, K C Tam^{64b}, N M Tamir¹⁵¹, A Tanaka¹⁵³, J Tanaka¹⁵³,
R Tanaka⁶⁶, M Tanasini^{57b,57a}, Z Tao¹⁶⁴, S Tapia Araya^{137f}, S Tapprogge¹⁰⁰,
A Tarek Abouefadl Mohamed¹⁰⁷, S Tarem¹⁵⁰, K Tariq^{14a}, G Tarna^{102,27b}, G F Tartarelli^{71a},
P Tas¹³³, M Tasevsky¹³¹, E Tassi^{43b,43a}, A C Tate¹⁶², G Tateno¹⁵³, Y Tayalati^{35e,w},
G N Taylor¹⁰⁵, W Taylor^{156b}, A S Tee¹⁷⁰, R Teixeira De Lima¹⁴³, P Teixeira-Dias⁹⁵, J J Teoh¹⁵⁵,
K Terashi¹⁵³, J Terron⁹⁹, S Terzo¹³, M Testa⁵³, R J Teuscher^{155,x}, A Thaler⁷⁹, O Theiner⁵⁶,
N Themistokleous⁵², T Thevenaux-Pelzer¹⁰², O Thielmann¹⁷¹, D W Thomas⁹⁵, J P Thomas²⁰,
E A Thompson^{17a}, P D Thompson²⁰, E Thomson¹²⁸, Y Tian⁵⁵, V Tikhomirov^{37,a},
Yu A Tikhonov³⁷, S Timoshenko³⁷, D Timoshyn¹³³, E X L Ting¹, P Tipton¹⁷², S H Tlou^{33g},
A Tnourji⁴⁰, K Todome¹⁵⁴, S Todorova-Nova¹³³, S Todt⁵⁰, M Togawa⁸⁴, J Tojo⁸⁹, S Tokár^{28a},
K Tokushuku⁸⁴, O Toldaiev⁶⁸, R Tombs³², M Tomoto^{84,111}, L Tompkins^{143,n},
K W Topolnicki^{86b}, E Torrence¹²³, H Torres^{102,ab}, E Torró Pastor¹⁶³, M Toscani³⁰, C Toscirí³⁹,
M Tost¹¹, D R Tovey¹³⁹, A Traet¹⁶, I S Trandafir^{27b}, T Trefzger¹⁶⁶, A Tricoli²⁹, I M Trigger^{156a},
S Trincaz-Duvoid¹²⁷, D A Trischuk²⁶, B Trocmé⁶⁰, L Truong^{33c}, M Trzebinski⁸⁷, A Trzupek⁸⁷,
F Tsai¹⁴⁵, M Tsai¹⁰⁶, A Tsiamis^{152,e}, P V Tsiarehka³⁷, S Tsigaridas^{156a}, A Tsigotis^{152,s},
V Tsiskaridze¹⁵⁵, E G Tskhadadze^{149a}, M Tsopoulou¹⁵², Y Tsujikawa⁸⁸, I I Tsukerman³⁷,
V Tsulaia^{17a}, S Tsuno⁸⁴, K Tsurii¹¹⁸, D Tsybychev¹⁴⁵, Y Tu^{64b}, A Tudorache^{27b},
V Tudorache^{27b}, A N Tuna⁶¹, S Turchikhin^{57b,57a}, I Turk Cakir^{3a}, R Turra^{71a}, T Turtuvshin^{38,y},
P M Tuts⁴¹, S Tzamarias^{152,e}, P Tzani¹⁰, E Tzovara¹⁰⁰, F Ukegawa¹⁵⁷,
P A Ulloa Poblete^{137c,137b}, E N Umaka²⁹, G Unal³⁶, M Unal¹¹, A Undrus²⁹, G Unel¹⁵⁹,
J Urban^{28b}, P Urquijo¹⁰⁵, P Urrejola^{137a}, G Usai⁸, R Ushioda¹⁵⁴, M Usman¹⁰⁸, Z Uysal⁸²,
V Vacek¹³², B Vachon¹⁰⁴, K O H Vadla¹²⁵, T Vafeiadis³⁶, A Vaitkus⁹⁶, C Valderanis¹⁰⁹,
E Valdes Santurio^{47a,47b}, M Valente^{156a}, S Valentineti^{23b,23a}, A Valero¹⁶³, E Valiente Moreno¹⁶³,
A Vallier^{102,ab}, J A Valls Ferrer¹⁶³, D R Van Arneman¹¹⁴, T R Van Daalen¹³⁸, A Van Der Graaf⁴⁹,
P Van Gemmeren⁶, M Van Rijnbach¹²⁵, S Van Stroud⁹⁶, I Van Vulpen¹¹⁴, M Vanadia^{76a,76b},
W Vandelli³⁶, E R Vandewall¹²¹, D Vannicola¹⁵¹, L Vannoli^{57b,57a}, R Vari^{75a}, E W Varnes⁷,
C Varni^{17b}, T Varol¹⁴⁸, D Varouchas⁶⁶, L Varriale¹⁶³, K E Varvell¹⁴⁷, M E Vasile^{27b}, L Vaslin⁸⁴,
G A Vasquez¹⁶⁵, A Vasyukov³⁸, R Vavricka¹⁰⁰, F Vazeille⁴⁰, T Vazquez Schroeder³⁶, J Veatch³¹,
V Vecchio¹⁰¹, M J Veen¹⁰³, I Veliscek¹²⁶, L M Veloce¹⁵⁵, F Veloso^{130a,130c}, S Veneziano^{75a},
A Ventura^{70a,70b}, S Ventura Gonzalez¹³⁵, A Verbitskyi¹¹⁰, M Verducci^{74a,74b}, C Vergis²⁴,
M Verissimo De Araujo^{83b}, W Verkerke¹¹⁴, J C Vermeulen¹¹⁴, C Vernieri¹⁴³, M Vessella¹⁰³,
M C Vetterli^{142,ag}, A Vgenopoulos^{152,e}, N Vieux Maira^{137f}, T Vickey¹³⁹, O E Vickey Boeriu¹³⁹,
G H A Viehhauser¹²⁶, L Vigani^{63b}, M Villa^{23b,23a}, M Villaplana Perez¹⁶³, E M Villhauer⁵²,
E Vilucchi⁵³, M G Vincter³⁴, G S Virdee²⁰, A Vishwakarma⁵², A Visibile¹¹⁴, C Vittori³⁶,
I Vivarelli^{23b,23a}, E Voevodina¹¹⁰, F Vogel¹⁰⁹, J C Voigt⁵⁰, P Vokac¹³², Yu Volkotrub^{86a},
J Von Ahnen⁴⁸, E Von Toerne²⁴, B Vormwald³⁶, V Vorobel¹³³, K Vorobev³⁷, M Vos¹⁶³,
K Voss¹⁴¹, M Vozak¹¹⁴, L Vozdecky¹²⁰, N Vranjes¹⁵, M Vranjes Milosavljevic¹⁵,
M Vreeswijk¹¹⁴, N K Vu^{62d,62c}, R Vuillermet³⁶, O Vujanovic¹⁰⁰, I Vukotic³⁹, S Wada¹⁵⁷,
C Wagner¹⁰³, J M Wagner^{17a}, W Wagner¹⁷¹, S Wahdan¹⁷¹, H Wahlberg⁹⁰, M Wakida¹¹¹,
J Walder¹³⁴, R Walker¹⁰⁹, W Walkowiak¹⁴¹, A Wall¹²⁸, E J Wallin⁹⁸, T Wamorkar⁶,
A Z Wang¹³⁶, C Wang¹⁰⁰, C Wang¹¹, H Wang^{17a}, J Wang^{64c}, R -J Wang¹⁰⁰, R Wang⁶¹,
R Wang⁶, S M Wang¹⁴⁸, S Wang^{62b}, T Wang^{62a}, W T Wang⁸⁰, W Wang^{14a}, X Wang^{14c},
X Wang¹⁶², X Wang^{62c}, Y Wang^{62d}, Y Wang^{14c}, Z Wang¹⁰⁶, Z Wang^{62d,51,62c}, Z Wang¹⁰⁶,
A Warburton¹⁰⁴, R J Ward²⁰, N Warrack⁵⁹, S Waterhouse⁹⁵, A T Watson²⁰, H Watson⁵⁹,
M F Watson²⁰, E Watton^{59,134}, G Watts¹³⁸, B M Waugh⁹⁶, C Weber²⁹, H A Weber¹⁸,
M S Weber¹⁹, S M Weber^{63a}, C Wei^{62a}, Y Wei¹²⁶, A R Weidberg¹²⁶, E J Weik¹¹⁷,
J Weingarten⁴⁹, M Weirich¹⁰⁰, C Weiser⁵⁴, C J Wells⁴⁸, T Wenaus²⁹, B Wendland⁴⁹,
T Wengler³⁶, N S Wenke¹¹⁰, N Wermes²⁴, M Wessels^{63a}, A M Wharton⁹¹, A S White⁶¹,
A White⁸, M J White¹, D Whiteson¹⁵⁹, L Wickremasinghe¹²⁴, W Wiedenmann¹⁷⁰,
M Wielers¹³⁴, C Wiglesworth⁴², D J Wilbern¹²⁰, H G Wilkens³⁶, D M Williams⁴¹, H H Williams¹²⁸,
S Williams³², S Willocq¹⁰³, B J Wilson¹⁰¹, P J Windischhofer³⁹, F I Winkel³⁰, F Winklmeier¹²³,
B T Winter⁵⁴, J K Winter¹⁰¹, M Wittgen¹⁴³, M Wobisch⁹⁷, Z Wolffs¹¹⁴, J Wollrath¹⁵⁹,

M W Wolter⁸⁷ , H Wolters^{130a,130c} , E L Woodward⁴¹ , S D Worm⁴⁸ , B K Wosiek⁸⁷ ,
 K W Woźniak⁸⁷ , S Wozniowski⁵⁵ , K Wraight⁵⁹ , C Wu²⁰ , M Wu^{14d} , M Wu¹¹³ , S L Wu¹⁷⁰ ,
 X Wu⁵⁶ , Y Wu^{62a} , Z Wu¹³⁵ , J Wuerzinger^{110,ac} , T R Wyatt¹⁰¹ , B M Wynne⁵² , S Xella⁴² ,
 L Xia^{14c} , M Xia^{14b} , J Xiang^{64c} , M Xie^{62a} , X Xie^{62a} , S Xin^{14a,14e} , A Xiong¹²³ , J Xiong^{17a} ,
 D Xu^{14a} , H Xu^{62a} , L Xu^{62a} , R Xu¹²⁸ , T Xu¹⁰⁶ , Y Xu^{14b} , Z Xu⁵² , Z Xu^{14c} , B Yabsley¹⁴⁷ ,
 S Yacoob^{33a} , Y Yamaguchi¹⁵⁴ , E Yamashita¹⁵³ , H Yamauchi¹⁵⁷ , T Yamazaki^{17a} , Y Yamazaki⁸⁵ ,
 J Yan^{62c} , S Yan⁵⁹ , Z Yan¹⁰³ , H J Yang^{62c,62d} , H T Yang^{62a} , S Yang^{62a} , T Yang^{64c} , X Yang³⁶ ,
 X Yang^{14a} , Y Yang⁴⁴ , Y Yang^{62a} , Z Yang^{62a} , W-M Yao^{17a} , H Ye^{14c} , H Ye⁵⁵ , J Ye^{14a} , S Ye²⁹ ,
 X Ye^{62a} , Y Yeh⁹⁶ , I Yeletsikh³⁸ , B K Yeo^{17b} , M R Yexley⁹⁶ , P Yin⁴¹ , K Yorita¹⁶⁸ ,
 S Younas^{27b} , C J S Young³⁶ , C Young¹⁴³ , C Yu^{14a,14e} , Y Yu^{62a} , M Yuan¹⁰⁶ , R Yuan^{62b} ,
 L Yue⁹⁶ , M Zaazoua^{62a} , B Zabinski⁸⁷ , E Zaid⁵² , Z K Zak⁸⁷ , T Zakareishvili¹⁶³ , N Zakharchuk³⁴ ,
 S Zambito⁵⁶ , J A Zamora Saa^{137d,137b} , J Zang¹⁵³ , D Zanzi⁵⁴ , O Zaplatilek¹³² , C Zeitnitz¹⁷¹ ,
 H Zeng^{14a} , J C Zeng¹⁶² , D T Zenger Jr²⁶ , O Zenin³⁷ , T Ženis^{28a} , S Zenz⁹⁴ , S Zerradi^{35a} ,
 D Zerwas⁶⁶ , M Zhai^{14a,14e} , D F Zhang¹³⁹ , J Zhang^{62b} , J Zhang⁶ , K Zhang^{14a,14e} , L Zhang^{14c} ,
 P Zhang^{14a,14e} , R Zhang¹⁷⁰ , S Zhang¹⁰⁶ , S Zhang⁴⁴ , T Zhang¹⁵³ , X Zhang^{62c} , X Zhang^{62b} ,
 Y Zhang^{62c,5} , Y Zhang⁹⁶ , Y Zhang^{14c} , Z Zhang^{17a} , Z Zhang⁶⁶ , H Zhao¹³⁸ , T Zhao^{62b} ,
 Y Zhao¹³⁶ , Z Zhao^{62a} , A Zhemchugov³⁸ , J Zheng^{14c} , K Zheng¹⁶² , X Zheng^{62a} , Z Zheng¹⁴³ ,
 D Zhong¹⁶² , B Zhou¹⁰⁶ , H Zhou⁷ , N Zhou^{62c} , Y Zhou^{14c} , Y Zhou⁷ , C G Zhu^{62b} , J Zhu¹⁰⁶ ,
 Y Zhu^{62c} , Y Zhu^{62a} , X Zhuang^{14a} , K Zhukov³⁷ , N I Zimine³⁸ , J Zinsser^{63b} , M Ziolkowski¹⁴¹ ,
 L Živković¹⁵ , A Zoccoli^{23b,23a} , K Zoch⁶¹ , T G Zorbas¹³⁹ , O Zormpa⁴⁶ , W Zou⁴¹ ,
 L Zwalinski³⁶ .

¹ Department of Physics, University of Adelaide, Adelaide, Australia

² Department of Physics, University of Alberta, Edmonton, AB, Canada

³ (a) Department of Physics, Ankara University, Ankara; (b) Division of Physics, TOBB University of Economics and Technology, Ankara, Türkiye

⁴ LAPP, Université Savoie Mont Blanc, CNRS/IN2P3, Annecy, France

⁵ APC, Université Paris Cité, CNRS/IN2P3, Paris, France

⁶ High Energy Physics Division, Argonne National Laboratory, Argonne, IL, United States of America

⁷ Department of Physics, University of Arizona, Tucson, AZ, United States of America

⁸ Department of Physics, University of Texas at Arlington, Arlington, TX, United States of America

⁹ Physics Department, National and Kapodistrian University of Athens, Athens, Greece

¹⁰ Physics Department, National Technical University of Athens, Zografou, Greece

¹¹ Department of Physics, University of Texas at Austin, Austin, TX, United States of America

¹² Institute of Physics, Azerbaijan Academy of Sciences, Baku, Azerbaijan

¹³ Institut de Física d'Altes Energies (IFAE), Barcelona Institute of Science and Technology, Barcelona, Spain

¹⁴ (a) Institute of High Energy Physics, Chinese Academy of Sciences, Beijing; (b) Physics Department, Tsinghua University, Beijing; (c) Department of Physics, Nanjing University, Nanjing; (d) School of Science, Shenzhen Campus of Sun Yat-sen University; (e) University of Chinese Academy of Science (UCAS), Beijing, People's Republic of China

¹⁵ Institute of Physics, University of Belgrade, Belgrade, Serbia

¹⁶ Department for Physics and Technology, University of Bergen, Bergen, Norway

¹⁷ (a) Physics Division, Lawrence Berkeley National Laboratory, Berkeley, CA; (b) University of California, Berkeley, CA, United States of America

¹⁸ Institut für Physik, Humboldt Universität zu Berlin, Berlin, Germany

¹⁹ Albert Einstein Center for Fundamental Physics and Laboratory for High Energy Physics, University of Bern, Bern, Switzerland

²⁰ School of Physics and Astronomy, University of Birmingham, Birmingham, United Kingdom

²¹ (a) Department of Physics, Bogazici University, Istanbul; (b) Department of Physics Engineering, Gaziantep University, Gaziantep; (c) Department of Physics, Istanbul University, Istanbul, Türkiye

²² (a) Facultad de Ciencias y Centro de Investigaciones, Universidad Antonio Nariño, Bogotá;

(b) Departamento de Física, Universidad Nacional de Colombia, Bogotá, Colombia

²³ (a) Dipartimento di Fisica e Astronomia A. Righi, Università di Bologna, Bologna; (b) INFN Sezione di Bologna, Italy

²⁴ Physikalisches Institut, Universität Bonn, Bonn, Germany

²⁵ Department of Physics, Boston University, Boston, MA, United States of America

²⁶ Department of Physics, Brandeis University, Waltham, MA, United States of America

²⁷ (a) Transilvania University of Brasov, Brasov; (b) Horia Hulubei National Institute of Physics and Nuclear Engineering, Bucharest; (c) Department of Physics, Alexandru Ioan Cuza University of Iasi, Iasi; (d) National

- Institute for Research and Development of Isotopic and Molecular Technologies, Physics Department, Cluj-Napoca; ^(e)National University of Science and Technology Politehnica, Bucharest; ^(f)West University in Timisoara, Timisoara; ^(g)Faculty of Physics, University of Bucharest, Bucharest, Romania
- ²⁸ ^(a)Faculty of Mathematics, Physics and Informatics, Comenius University, Bratislava; ^(b)Department of Subnuclear Physics, Institute of Experimental Physics of the Slovak Academy of Sciences, Kosice, Slovakia
- ²⁹ Physics Department, Brookhaven National Laboratory, Upton, NY, United States of America
- ³⁰ Universidad de Buenos Aires, Facultad de Ciencias Exactas y Naturales, Departamento de Física, y CONICET, Instituto de Física de Buenos Aires (IFIBA), Buenos Aires, Argentina
- ³¹ California State University, CA, United States of America
- ³² Cavendish Laboratory, University of Cambridge, Cambridge, United Kingdom
- ³³ ^(a)Department of Physics, University of Cape Town, Cape Town; ^(b)iThemba Labs, Western Cape; ^(c)Department of Mechanical Engineering Science, University of Johannesburg, Johannesburg; ^(d)National Institute of Physics, University of the Philippines Diliman (Philippines); ^(e)University of South Africa, Department of Physics, Pretoria; ^(f)University of Zululand, KwaDlangezwa; ^(g)School of Physics, University of the Witwatersrand, Johannesburg, South Africa
- ³⁴ Department of Physics, Carleton University, Ottawa, ON, Canada
- ³⁵ ^(a)Faculté des Sciences Ain Chock, Réseau Universitaire de Physique des Hautes Energies—Université Hassan II, Casablanca; ^(b)Faculté des Sciences, Université Ibn-Tofail, Kénitra; ^(c)Faculté des Sciences Semlalia, Université Cadi Ayyad, LPHEA-Marrakech; ^(d)LPMR, Faculté des Sciences, Université Mohamed Premier, Oujda; ^(e)Faculté des sciences, Université Mohammed V, Rabat; ^(f)Institute of Applied Physics, Mohammed VI Polytechnic University, Ben Guerir, Morocco
- ³⁶ CERN Geneva, Switzerland
- ³⁷ Affiliated with an institute covered by a cooperation agreement with CERN
- ³⁸ Affiliated with an international laboratory covered by a cooperation agreement with CERN
- ³⁹ Enrico Fermi Institute, University of Chicago, Chicago, IL, United States of America
- ⁴⁰ LPC, Université Clermont Auvergne, CNRS/IN2P3, Clermont-Ferrand, France
- ⁴¹ Nevis Laboratory, Columbia University, Irvington, NY, United States of America
- ⁴² Niels Bohr Institute, University of Copenhagen, Copenhagen, Denmark
- ⁴³ ^(a)Dipartimento di Fisica, Università della Calabria, Rende; ^(b)INFN Gruppo Collegato di Cosenza, Laboratori Nazionali di Frascati, Italy
- ⁴⁴ Physics Department, Southern Methodist University, Dallas, TX, United States of America
- ⁴⁵ Physics Department, University of Texas at Dallas, Richardson, TX, United States of America
- ⁴⁶ National Centre for Scientific Research ‘Demokritos’, Agia Paraskevi, Greece
- ⁴⁷ ^(a)Department of Physics, Stockholm University; ^(b)Oskar Klein Centre, Stockholm, Sweden
- ⁴⁸ Deutsches Elektronen-Synchrotron DESY, Hamburg and Zeuthen, Germany
- ⁴⁹ Fakultät Physik, Technische Universität Dortmund, Dortmund, Germany
- ⁵⁰ Institut für Kern- und Teilchenphysik, Technische Universität Dresden, Dresden, Germany
- ⁵¹ Department of Physics, Duke University, Durham, NC, United States of America
- ⁵² SUPA—School of Physics and Astronomy, University of Edinburgh, Edinburgh, United Kingdom
- ⁵³ INFN e Laboratori Nazionali di Frascati, Frascati, Italy
- ⁵⁴ Physikalisches Institut, Albert-Ludwigs-Universität Freiburg, Freiburg, Germany
- ⁵⁵ II. Physikalisches Institut, Georg-August-Universität Göttingen, Göttingen, Germany
- ⁵⁶ Département de Physique Nucléaire et Corpusculaire, Université de Genève, Genève, Switzerland
- ⁵⁷ ^(a)Dipartimento di Fisica, Università di Genova, Genova; ^(b)INFN Sezione di Genova, Italy
- ⁵⁸ II. Physikalisches Institut, Justus-Liebig-Universität Giessen, Giessen, Germany
- ⁵⁹ SUPA—School of Physics and Astronomy, University of Glasgow, Glasgow, United Kingdom
- ⁶⁰ LPSC, Université Grenoble Alpes, CNRS/IN2P3, Grenoble INP, Grenoble, France
- ⁶¹ Laboratory for Particle Physics and Cosmology, Harvard University, Cambridge, MA, United States of America
- ⁶² ^(a)Department of Modern Physics and State Key Laboratory of Particle Detection and Electronics, University of Science and Technology of China, Hefei; ^(b)Institute of Frontier and Interdisciplinary Science and Key Laboratory of Particle Physics and Particle Irradiation (MOE), Shandong University, Qingdao; ^(c)School of Physics and Astronomy, Shanghai Jiao Tong University, Key Laboratory for Particle Astrophysics and Cosmology (MOE), SKLPPC, Shanghai; ^(d)Tsung-Dao Lee Institute, Shanghai; ^(e)School of Physics and Microelectronics, Zhengzhou University, People’s Republic of China
- ⁶³ ^(a)Kirchhoff-Institut für Physik, Ruprecht-Karls-Universität Heidelberg, Heidelberg; ^(b)Physikalisches Institut, Ruprecht-Karls-Universität Heidelberg, Heidelberg, Germany
- ⁶⁴ ^(a)Department of Physics, Chinese University of Hong Kong, Shatin, N.T., Hong Kong Special Administrative Region of China; ^(b)Department of Physics, University of Hong Kong, Hong

- Kong;^(c) Department of Physics and Institute for Advanced Study, Hong Kong University of Science and Technology, Clear Water Bay, Kowloon, Hong Kong Special Administrative Region of China, People's Republic of China
- ⁶⁵ Department of Physics, National Tsing Hua University, Hsinchu, Taiwan
- ⁶⁶ IJCLab, Université Paris-Saclay, CNRS/IN2P3, 91 405, Orsay, France
- ⁶⁷ Centro Nacional de Microelectrónica (IMB-CNM-CSIC), Barcelona, Spain
- ⁶⁸ Department of Physics, Indiana University, Bloomington, IN, United States of America
- ⁶⁹ ^(a) INFN Gruppo Collegato di Udine, Sezione di Trieste, Udine; ^(b) ICTP, Trieste; ^(c) Dipartimento Politecnico di Ingegneria e Architettura, Università di Udine, Udine, Italy
- ⁷⁰ ^(a) INFN Sezione di Lecce; ^(b) Dipartimento di Matematica e Fisica, Università del Salento, Lecce, Italy
- ⁷¹ ^(a) INFN Sezione di Milano; ^(b) Dipartimento di Fisica, Università di Milano, Milano, Italy
- ⁷² ^(a) INFN Sezione di Napoli; ^(b) Dipartimento di Fisica, Università di Napoli, Napoli, Italy
- ⁷³ ^(a) INFN Sezione di Pavia; ^(b) Dipartimento di Fisica, Università di Pavia, Pavia, Italy
- ⁷⁴ ^(a) INFN Sezione di Pisa; ^(b) Dipartimento di Fisica E. Fermi, Università di Pisa, Pisa, Italy
- ⁷⁵ ^(a) INFN Sezione di Roma; ^(b) Dipartimento di Fisica, Sapienza Università di Roma, Roma, Italy
- ⁷⁶ ^(a) INFN Sezione di Roma Tor Vergata; ^(b) Dipartimento di Fisica, Università di Roma Tor Vergata, Roma, Italy
- ⁷⁷ ^(a) INFN Sezione di Roma Tre; ^(b) Dipartimento di Matematica e Fisica, Università Roma Tre, Roma, Italy
- ⁷⁸ ^(a) INFN-TIFPA; ^(b) Università degli Studi di Trento, Trento, Italy
- ⁷⁹ Universität Innsbruck, Department of Astro and Particle Physics, Innsbruck, Austria
- ⁸⁰ University of Iowa, Iowa City, IA, United States of America
- ⁸¹ Department of Physics and Astronomy, Iowa State University, Ames, IA, United States of America
- ⁸² Istinye University, Sariyer, Istanbul, Türkiye
- ⁸³ ^(a) Departamento de Engenharia Elétrica, Universidade Federal de Juiz de Fora (UFJF), Juiz de Fora; ^(b) Universidade Federal do Rio De Janeiro COPPE/EE/IF, Rio de Janeiro; ^(c) Instituto de Física, Universidade de São Paulo, São Paulo; ^(d) Rio de Janeiro State University, Rio de Janeiro, Brazil
- ⁸⁴ KEK, High Energy Accelerator Research Organization, Tsukuba, Japan
- ⁸⁵ Graduate School of Science, Kobe University, Kobe, Japan
- ⁸⁶ ^(a) AGH University of Krakow, Faculty of Physics and Applied Computer Science, Krakow; ^(b) Marian Smoluchowski Institute of Physics, Jagiellonian University, Krakow, Poland
- ⁸⁷ Institute of Nuclear Physics Polish Academy of Sciences, Krakow, Poland
- ⁸⁸ Faculty of Science, Kyoto University, Kyoto, Japan
- ⁸⁹ Research Center for Advanced Particle Physics and Department of Physics, Kyushu University, Fukuoka, Japan
- ⁹⁰ Instituto de Física La Plata, Universidad Nacional de La Plata and CONICET, La Plata, Argentina
- ⁹¹ Physics Department, Lancaster University, Lancaster, United Kingdom
- ⁹² Oliver Lodge Laboratory, University of Liverpool, Liverpool, United Kingdom
- ⁹³ Department of Experimental Particle Physics, Jožef Stefan Institute and Department of Physics, University of Ljubljana, Ljubljana, Slovenia
- ⁹⁴ School of Physics and Astronomy, Queen Mary University of London, London, United Kingdom
- ⁹⁵ Department of Physics, Royal Holloway University of London, Egham, United Kingdom
- ⁹⁶ Department of Physics and Astronomy, University College London, London, United Kingdom
- ⁹⁷ Louisiana Tech University, Ruston, LA, United States of America
- ⁹⁸ Fysiska institutionen, Lunds universitet, Lund, Sweden
- ⁹⁹ Departamento de Física Teórica C-15 and CIAFF, Universidad Autónoma de Madrid, Madrid, Spain
- ¹⁰⁰ Institut für Physik, Universität Mainz, Mainz, Germany
- ¹⁰¹ School of Physics and Astronomy, University of Manchester, Manchester, United Kingdom
- ¹⁰² CPPM, Aix-Marseille Université, CNRS/IN2P3, Marseille, France
- ¹⁰³ Department of Physics, University of Massachusetts, Amherst, MA, United States of America
- ¹⁰⁴ Department of Physics, McGill University, Montreal, QC, Canada
- ¹⁰⁵ School of Physics, University of Melbourne, Victoria, Australia
- ¹⁰⁶ Department of Physics, University of Michigan, Ann Arbor, MI, United States of America
- ¹⁰⁷ Department of Physics and Astronomy, Michigan State University, East Lansing, MI, United States of America
- ¹⁰⁸ Group of Particle Physics, University of Montreal, Montreal, QC, Canada
- ¹⁰⁹ Fakultät für Physik, Ludwig-Maximilians-Universität München, München, Germany
- ¹¹⁰ Max-Planck-Institut für Physik (Werner-Heisenberg-Institut), München, Germany
- ¹¹¹ Graduate School of Science and Kobayashi-Maskawa Institute, Nagoya University, Nagoya, Japan

- ¹¹² Department of Physics and Astronomy, University of New Mexico, Albuquerque, NM, United States of America
- ¹¹³ Institute for Mathematics, Astrophysics and Particle Physics, Radboud University/Nikhef, Nijmegen, The Netherlands
- ¹¹⁴ Nikhef National Institute for Subatomic Physics and University of Amsterdam, Amsterdam, The Netherlands
- ¹¹⁵ Department of Physics, Northern Illinois University, DeKalb, IL, United States of America
- ¹¹⁶ ^(a)New York University Abu Dhabi, Abu Dhabi; ^(b)United Arab Emirates University, Al Ain, United Arab Emirates
- ¹¹⁷ Department of Physics, New York University, New York, NY, United States of America
- ¹¹⁸ Ochanomizu University, Otsuka, Bunkyo-ku, Tokyo, Japan
- ¹¹⁹ Ohio State University, Columbus, OH, United States of America
- ¹²⁰ Homer L. Dodge Department of Physics and Astronomy, University of Oklahoma, Norman, OK, United States of America
- ¹²¹ Department of Physics, Oklahoma State University, Stillwater, OK, United States of America
- ¹²² Palacký University, Joint Laboratory of Optics, Olomouc, Czech Republic
- ¹²³ Institute for Fundamental Science, University of Oregon, Eugene, OR, United States of America
- ¹²⁴ Graduate School of Science, Osaka University, Osaka, Japan
- ¹²⁵ Department of Physics, University of Oslo, Oslo, Norway
- ¹²⁶ Department of Physics, Oxford University, Oxford, United Kingdom
- ¹²⁷ LPNHE, Sorbonne Université, Université Paris Cité, CNRS/IN2P3, Paris, France
- ¹²⁸ Department of Physics, University of Pennsylvania, Philadelphia, PA, United States of America
- ¹²⁹ Department of Physics and Astronomy, University of Pittsburgh, Pittsburgh, PA, United States of America
- ¹³⁰ ^(a)Laboratório de Instrumentação e Física Experimental de Partículas—LIP, Lisboa; ^(b)Departamento de Física, Faculdade de Ciências, Universidade de Lisboa, Lisboa; ^(c)Departamento de Física, Universidade de Coimbra, Coimbra; ^(d)Centro de Física Nuclear da Universidade de Lisboa, Lisboa; ^(e)Departamento de Física, Universidade do Minho, Braga; ^(f)Departamento de Física Teórica y del Cosmos, Universidad de Granada, Granada (Spain); ^(g)Departamento de Física, Instituto Superior Técnico, Universidade de Lisboa, Lisboa, Portugal
- ¹³¹ Institute of Physics of the Czech Academy of Sciences, Prague, Czech Republic
- ¹³² Czech Technical University in Prague, Prague, Czech Republic
- ¹³³ Charles University, Faculty of Mathematics and Physics, Prague, Czech Republic
- ¹³⁴ Particle Physics Department, Rutherford Appleton Laboratory, Didcot, United Kingdom
- ¹³⁵ IRFU, CEA, Université Paris-Saclay, Gif-sur-Yvette, France
- ¹³⁶ Santa Cruz Institute for Particle Physics, University of California Santa Cruz, Santa Cruz, CA, United States of America
- ¹³⁷ ^(a)Departamento de Física, Pontificia Universidad Católica de Chile, Santiago; ^(b)Millennium Institute for Subatomic physics at high energy frontier (SAPHIR), Santiago; ^(c)Instituto de Investigación Multidisciplinario en Ciencia y Tecnología, y Departamento de Física, Universidad de La Serena; ^(d)Universidad Andres Bello, Department of Physics, Santiago; ^(e)Instituto de Alta Investigación, Universidad de Tarapacá, Arica; ^(f)Departamento de Física, Universidad Técnica Federico Santa María, Valparaíso, Chile
- ¹³⁸ Department of Physics, University of Washington, Seattle, WA, United States of America
- ¹³⁹ Department of Physics and Astronomy, University of Sheffield, Sheffield, United Kingdom
- ¹⁴⁰ Department of Physics, Shinshu University, Nagano, Japan
- ¹⁴¹ Department Physik, Universität Siegen, Siegen, Germany
- ¹⁴² Department of Physics, Simon Fraser University, Burnaby, BC, Canada
- ¹⁴³ SLAC National Accelerator Laboratory, Stanford, CA, United States of America
- ¹⁴⁴ Department of Physics, Royal Institute of Technology, Stockholm, Sweden
- ¹⁴⁵ Departments of Physics and Astronomy, Stony Brook University, Stony Brook, NY, United States of America
- ¹⁴⁶ Department of Physics and Astronomy, University of Sussex, Brighton, United Kingdom
- ¹⁴⁷ School of Physics, University of Sydney, Sydney, Australia
- ¹⁴⁸ Institute of Physics, Academia Sinica, Taipei, Taiwan
- ¹⁴⁹ ^(a)E. Andronikashvili Institute of Physics, Iv. Javakhishvili Tbilisi State University, Tbilisi; ^(b)High Energy Physics Institute, Tbilisi State University, Tbilisi; ^(c)University of Georgia, Tbilisi, Georgia
- ¹⁵⁰ Department of Physics, Technion, Israel Institute of Technology, Haifa, Israel
- ¹⁵¹ Raymond and Beverly Sackler School of Physics and Astronomy, Tel Aviv University, Tel Aviv, Israel
- ¹⁵² Department of Physics, Aristotle University of Thessaloniki, Thessaloniki, Greece

- ¹⁵³ International Center for Elementary Particle Physics and Department of Physics, University of Tokyo, Tokyo, Japan
- ¹⁵⁴ Department of Physics, Tokyo Institute of Technology, Tokyo, Japan
- ¹⁵⁵ Department of Physics, University of Toronto, Toronto, ON, Canada
- ¹⁵⁶ (a) TRIUMF, Vancouver BC; (b) Department of Physics and Astronomy, York University, Toronto, ON, Canada
- ¹⁵⁷ Division of Physics and Tomonaga Center for the History of the Universe, Faculty of Pure and Applied Sciences, University of Tsukuba, Tsukuba, Japan
- ¹⁵⁸ Department of Physics and Astronomy, Tufts University, Medford, MA, United States of America
- ¹⁵⁹ Department of Physics and Astronomy, University of California Irvine, Irvine, CA, United States of America
- ¹⁶⁰ University of Sharjah, Sharjah, United Arab Emirates
- ¹⁶¹ Department of Physics and Astronomy, University of Uppsala, Uppsala, Sweden
- ¹⁶² Department of Physics, University of Illinois, Urbana, IL, United States of America
- ¹⁶³ Instituto de Física Corpuscular (IFIC), Centro Mixto Universidad de Valencia—CSIC, Valencia, Spain
- ¹⁶⁴ Department of Physics, University of British Columbia, Vancouver, BC, Canada
- ¹⁶⁵ Department of Physics and Astronomy, University of Victoria, Victoria, BC, Canada
- ¹⁶⁶ Fakultät für Physik und Astronomie, Julius-Maximilians-Universität Würzburg, Würzburg, Germany
- ¹⁶⁷ Department of Physics, University of Warwick, Coventry, United Kingdom
- ¹⁶⁸ Waseda University, Tokyo, Japan
- ¹⁶⁹ Department of Particle Physics and Astrophysics, Weizmann Institute of Science, Rehovot, Israel
- ¹⁷⁰ Department of Physics, University of Wisconsin, Madison, WI, United States of America
- ¹⁷¹ Fakultät für Mathematik und Naturwissenschaften, Fachgruppe Physik, Bergische Universität Wuppertal, Wuppertal, Germany
- ¹⁷² Department of Physics, Yale University, New Haven, CT, United States of America
- ^a Also Affiliated with an institute covered by a cooperation agreement with CERN.
- ^b Also at An-Najah National University, Nablus, Palestine.
- ^c Also at Borough of Manhattan Community College, City University of New York, New York, NY, United States of America.
- ^d Also at Center for High Energy Physics, Peking University, People's Republic of China.
- ^e Also at Center for Interdisciplinary Research and Innovation (CIRI-AUTH), Thessaloniki, Greece.
- ^f Also at Centro Studi e Ricerche Enrico Fermi, Italy.
- ^g Also at CERN Geneva, Switzerland.
- ^h Also at Département de Physique Nucléaire et Corpusculaire, Université de Genève, Genève, Switzerland.
- ⁱ Also at Departament de Física de la Universitat Autònoma de Barcelona, Barcelona, Spain.
- ^j Also at Department of Financial and Management Engineering, University of the Aegean, Chios, Greece.
- ^k Also at Department of Physics, Ben Gurion University of the Negev, Beer Sheva, Israel.
- ^l Also at Department of Physics, California State University, Sacramento, United States of America.
- ^m Also at Department of Physics, King's College London, London, United Kingdom.
- ⁿ Also at Department of Physics, Stanford University, Stanford, CA, United States of America.
- ^o Also at Department of Physics, Stellenbosch University, South Africa.
- ^p Also at Department of Physics, University of Fribourg, Fribourg, Switzerland.
- ^q Also at Department of Physics, University of Thessaly, Greece.
- ^r Also at Department of Physics, Westmont College, Santa Barbara, United States of America.
- ^s Also at Hellenic Open University, Patras, Greece.
- ^t Also at Institutio Catalana de Recerca i Estudis Avancats, ICREA, Barcelona, Spain.
- ^u Also at Institut für Experimentalphysik, Universität Hamburg, Hamburg, Germany.
- ^v Also at Institute for Nuclear Research and Nuclear Energy (INRNE) of the Bulgarian Academy of Sciences, Sofia, Bulgaria.
- ^w Also at Institute of Applied Physics, Mohammed VI Polytechnic University, Ben Guerir, Morocco.
- ^x Also at Institute of Particle Physics (IPP), Canada.
- ^y Also at Institute of Physics and Technology, Mongolian Academy of Sciences, Ulaanbaatar, Mongolia.
- ^z Also at Institute of Physics, Azerbaijan Academy of Sciences, Baku, Azerbaijan.
- ^{aa} Also at Institute of Theoretical Physics, Ilia State University, Tbilisi, Georgia.
- ^{ab} Also at L2IT, Université de Toulouse, CNRS/IN2P3, UPS, Toulouse, France.
- ^{ac} Also at Lawrence Livermore National Laboratory, Livermore, United States of America.
- ^{ad} Also at National Institute of Physics, University of the Philippines Diliman (Philippines), Philippines.
- ^{ae} Also at Technical University of Munich, Munich, Germany.

- ^{af} Also at The Collaborative Innovation Center of Quantum Matter (CICQM), Beijing, People's Republic of China.
- ^{ag} Also at TRIUMF, Vancouver, BC, Canada.
- ^{ah} Also at Università di Napoli Parthenope, Napoli, Italy.
- ^{ai} Also at University of Colorado Boulder, Department of Physics, Colorado, United States of America.
- ^{aj} Also at Washington College, Chestertown, MD, United States of America.
- ^{ak} Also at Yeditepe University, Physics Department, Istanbul, Türkiye.
- [†] Deceased.

ORCID iD

The ATLAS Collaboration  <https://orcid.org/0000-0002-5108-0042>

References

- [1] Gross F *et al* 2022 50 years of quantum chromodynamics (arXiv:2212.11107 [hep-ph])
- [2] ATLAS Collaboration 2021 Jet energy scale and resolution measured in proton–proton collisions at $\sqrt{s} = 13$ TeV with the ATLAS detector *Eur. Phys. J. C* **81** 689
- [3] CMS Collaboration 2021 Jet energy scale and resolution measurement with Run 2 Legacy Data Collected by CMS at 13 TeV (CMS-DP-2021-033) (available at: <https://cds.cern.ch/record/2792322>)
- [4] ATLAS Collaboration 2008 The ATLAS experiment at the CERN Large Hadron Collider *J. Instrum.* **3** S08003
- [5] ATLAS Collaboration 2010 *ATLAS Insertable B-Layer Technical Design Report* (ATLAS-TDR-19; CERN-LHCC-2010-013) (Available at: <https://cds.cern.ch/record/1291633>) ATLAS Collaboration 2010 *ATLAS Insertable B-Layer Technical Design Report Addendum* (ATLAS-TDR-19-ADD-1; CERN-LHCC-2012-009) (available at: <https://cds.cern.ch/record/1451888>)
- [6] Abbott B *et al* 2018 Production and integration of the ATLAS Insertable B-Layer *J. Instrum.* **13** T05008
- [7] ATLAS Collaboration 2021 The ATLAS collaboration software and firmware (ATL-SOFT-PUB-2021-001) (available at: <https://cds.cern.ch/record/2767187>)
- [8] ATLAS Collaboration 2010 The ATLAS Inner Detector commissioning and calibration *Eur. Phys. J. C* **70** 787
- [9] ATLAS Collaboration 2017 Performance of the ATLAS track reconstruction algorithms in dense environments in LHC Run 2 *Eur. Phys. J. C* **77** 673
- [10] ATLAS Collaboration 2017 Topological cell clustering in the ATLAS calorimeters and its performance in LHC Run 1 *Eur. Phys. J. C* **77** 490
- [11] ATLAS Collaboration 2017 Jet reconstruction and performance using particle flow with the ATLAS Detector *Eur. Phys. J. C* **77** 466
- [12] ATLAS Collaboration 2017 Improving jet substructure performance in ATLAS using Track-CaloClusters (ATL-PHYS-PUB-2017-015) (available at: <https://cds.cern.ch/record/2275636>)
- [13] Cukierman A and Nachman B 2017 Mathematical properties of numerical inversion for jet calibrations *Nucl. Instrum. Methods Phys. Res. A* **858** 1–11
- [14] ATLAS Collaboration 2013 Jet energy measurement with the ATLAS detector in proton–proton collisions at $\sqrt{s} = 7$ TeV *Eur. Phys. J. C* **73** 2304
- [15] ATLAS Collaboration 2018 Generalized numerical inversion: a neutral network approach to jet calibration (ATL-PHYS-PUB-2018-013) (available at: <https://cds.cern.ch/record/2630972>)
- [16] ATLAS Collaboration 2023 New techniques for jet calibration with the ATLAS detector *Eur. Phys. J. C* **83** 761
- [17] Agostinelli S 2003 GEANT4—a simulation toolkit *Nucl. Instrum. Methods Phys. Res. A* **506** 250–303
- [18] ATLAS Collaboration 2010 The ATLAS simulation infrastructure *Eur. Phys. J. C* **70** 823
- [19] Sjöstrand T, Ask S, Christiansen J R, Corke R, Desai N, Ilten P, Mrenna S, Prestel S, Rasmussen C O and Skands P Z 2015 An introduction to PYTHIA 8.2 *Comput. Phys. Commun.* **191** 159
- [20] Ball R D *et al* NNPDF Collaboration 2013 Parton distributions with LHC data *Nucl. Phys. B* **867** 244
- [21] ATLAS Collaboration 2014 ATLAS Pythia 8 tunes to 7 TeV data (ATL-PHYS-PUB-2014-021) (available at: <https://cds.cern.ch/record/1966419>)
- [22] Randall L and Sundrum R 1999 Large mass hierarchy from a small extra dimension *Phys. Rev. Lett.* **83** 3370–3
- [23] Bothmann E *et al* 2019 Event generation with Sherpa 2.2 *SciPost Phys.* **7** 034
- [24] Schumann S and Krauss F 2008 A parton shower algorithm based on Catani–Seymour dipole factorisation *J. High Energy Phys.* **JHEP03(2008)038**
- [25] Dulat S, Hou T -J, Gao J, Guzzi M, Huston J, Nadolsky P, Pumplin J, Schmidt C, Stump D and Yuan C P 2016 New parton distribution functions from a global analysis of quantum chromodynamics *Phys. Rev. D* **93** 033006
- [26] Winter J -C, Krauss F and Soff G 2004 A modified cluster-hadronisation model *Eur. Phys. J. C* **36** 381–95
- [27] Sjöstrand T, Mrenna S and Skands P 2008 A brief introduction to PYTHIA 8.1 *Comput. Phys. Commun.* **178** 852–67
- [28] ATLAS Collaboration 2016 The Pythia 8 A3 tune description of ATLAS minimum bias and inelastic measurements incorporating the Donnachie–Landshoff diffractive model (ATL-PHYS-PUB-2016-017) (available at: <https://cds.cern.ch/record/2206965>)
- [29] ATLAS Collaboration 2021 Optimisation of large-radius jet reconstruction for the ATLAS detector in 13 TeV proton–proton collisions *Eur. Phys. J. C* **81** 334
- [30] Cacciari M, Salam G P and Soyez G 2008 The anti- k_r jet clustering algorithm *J. High Energy Phys.* **JHEP04(2008)063**
- [31] Cacciari M, Salam G P and Soyez G 2012 FastJet user manual *Eur. Phys. J. C* **72** 1896
- [32] Dasgupta M, Fregoso A, Marzani S and Salam G P 2013 Towards an understanding of jet substructure *J. High Energy Phys.* **JHEP09(2013)029**
- [33] Cheong S, Cukierman A, Nachman B, Safdari M and Schwartzman A 2020 Parametrizing the detector response with neural networks *J. Instrum.* **15** 01030
- [34] ATLAS Collaboration 2019 Performance of top–quark and W -boson tagging with ATLAS in Run 2 of the LHC *Eur. Phys. J. C* **79** 375
- [35] Thaler J and Wang L -T 2008 Strategies to identify boosted tops *J. High Energy Phys.* **JHEP07(2008)092**
- [36] Larkoski A J, Salam G P and Thaler J 2013 Energy correlation functions for jet substructure *J. High Energy Phys.* **JHEP06(2013)108**

- [37] Larkoski A J, Moult I and Neill D 2014 Power counting to better jet observables *J. High Energy Phys.* [JHEP12\(2014\)009](#)
- [38] Thaler J and Van Tilburg K 2011 Identifying boosted objects with N-subjettiness *J. High Energy Phys.* [JHEP03\(2011\)015](#)
- [39] Larkoski A J, Neill D and Thaler J 2014 Jet shapes with the broadening axis *J. High Energy Phys.* [JHEP04\(2014\)017](#)
- [40] He K, Zhang X, Ren S and Sun J 2015 Deep residual learning for image recognition *CoRR* (arXiv:[1512.03385](#))
- [41] Misra D 2019 Mish: a self regularized non-monotonic neural activation function *CoRR* (arXiv:[1908.08681](#))
- [42] Liu L 2019 On the variance of the adaptive learning rate and beyond *CoRR* (arXiv:[1908.03265](#))
- [43] Dubey S R 2019 diffGrad: an optimization method for convolutional neural networks *CoRR* (arXiv:[1909.11015](#))
- [44] Savitzky A and Golay M J E 1964 Smoothing and differentiation of data by simplified least squares procedures *Anal. Chem.* **36** 1627–39
- [45] Nanda N, Chan L, Lieberum T, Smith J and Steinhardt J 2023 Progress measures for grokking via mechanistic interpretability *11th Int. Conf. on Learning Representations* (arXiv:[2301.05217](#))
- [46] Lundberg S M and Lee S-I 2017 A unified approach to interpreting model predictions *Advances in Neural Information Processing Systems* vol 30
- [47] ATLAS Collaboration 2023 ATLAS computing acknowledgements (ATL-SOFT-PUB-2023-001) (Available at: <https://cds.cern.ch/record/2869272>)